Development and Assessment of Pressure-Based and Model-Based Techniques for the MFB50 Control of a Euro VI 3.0L Diesel Engine

CHEMISTRY
A European Journal

www.chemeurj.org

A Journal of

ChemPubSoc Europe

2018-24/47

YC

Young Chemists Special Issue

In honor of young researchers around the world including the recent finalists of the European Young Chemist Award (EYCA)

Supported by

ACES Asian Chemical Editorial Society

WILEY-VCH

ChemPubSoc Europe

DOI: 10.1002/chem.201801096

CHEMISTRY
A European Journal
Review

Photovoltaic Doping

Caesium for Perovskite Solar Cells: An Overview

Federico Bella,*[a] Polyssena Renzi,*[b] Carmen Cavallo,*[c] and Claudio Gerbaldi*[a]

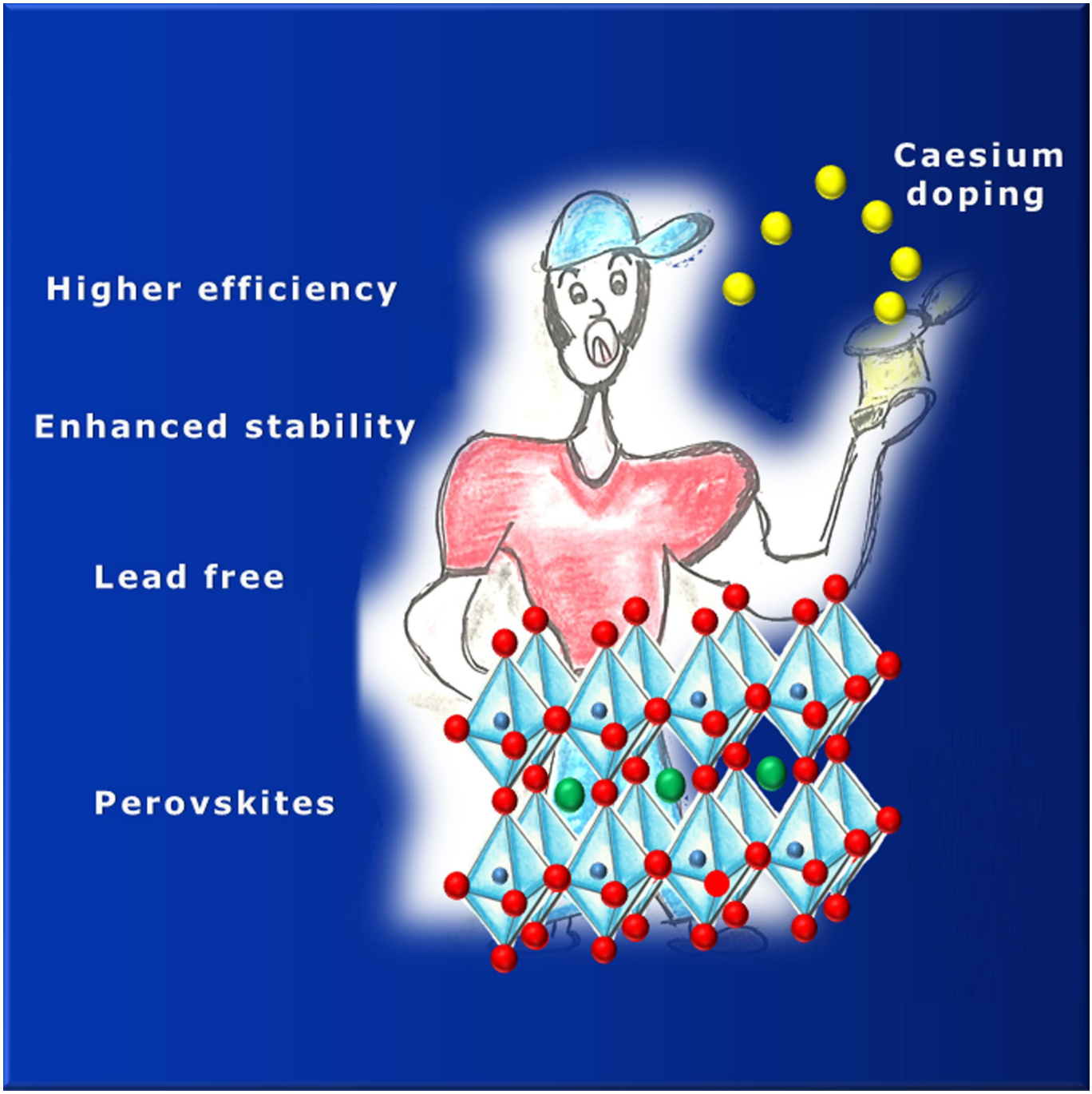

Abstract: Perovskite solar cells have the potential to revolutionize the world of photovoltaics, and their efficiency close to 23% on a lab-scale recently certified this novel technology as the one with the most rapidly raising performance per year in the whole story of solar cells. With the aim of improving stability, reproducibility and spectral properties of the devices, in the last three years the scientific community strongly focused on Cs-doping for hybrid (typically, organo-lead) perovskites. In parallel, to further contrast hygroscopicity and reach thermal stability, research has also been carried out to achieve the development of all-inorganic perovskites based on caesium, the performances of which are rapidly increasing. The potential of caesium is further strengthened when it is used as a modifying agent of charge-carrier layers in solar cells, but also for the preparation of perovskites with peculiar optoelectronic properties for unconventional applications (e.g., in LEDs, photodetectors, sensors, etc.). This Review offers a 360-degree overview on how caesium can strongly tune the properties and performance of perovskites and relative perovskite-based devices.

Introduction

Perovskite solar cells (PSCs) represent the currently most-studied photovoltaic technology.[1–10] After about five years from their initial discovery, these solar cells recorded a year-by-year growth rate of their efficiency values never provided by other technologies.[11–20] The current research activity in the optimisation of device architecture, materials and interfaces makes the future commercialization and exploitation of PSCs truly concrete and intriguing.[21–27]

The architecture of a PSC is rather simple in its standard configuration: a conductive glass (or a plastic foil) supports an electron extraction layer (ETL, such as TiO_2 or ZnO), on the top of which the perovskite-based active material is deposited. A hole-transporting material (HTM) is coated onto the perovskite layer, whereas back-contacts (typically gold or carbon-based) are evaporated/printed at the top of the cell.[28–32] Under sunlight, charge-generation is induced, and both positive and negative charge carriers are transported through the perovskite nanostructure to ETL/HTM charge selective contacts.[33–37] The core component of this solar cell is the perovskite active material, bearing a generic structure ABX_3, in which A is a monovalent cation (like methylammonium $CH_3NH_3^+$ or MA, formamidinium $CH_2(NH_2)_2^+$ or FA, Cs^+, Rb^+), B stands for Pb^{II} or Sn^{II} and X for I or Br.[38–42] The outstanding optoelectronic properties of perovskites, characterized by high mobility and absorption coefficient, long-balanced carrier diffusion length and low-exciton binding energy, justify the current success of this photovoltaic technology.[43–47] Several review articles have been published on different strategies to improve the performance of lab-scale PSCs.[48–57]

As it is typical for novel technologies,[58–62] research in the field of PSCs is currently focused on overcoming important issues, starting from the difficulty of reproducing high power conversion efficiency (PCE) values when the device area is increased at the module level. Secondly, the selection of cell components must be reconsidered thinking at a large-scale commercialization because some of the standard materials (like HTMs) currently used in lab-scale devices have unrealistic costs for a third generation photovoltaic technology.[63] The versatility of perovskites has been further enriched in the last years because it has been shown that they present tuneable properties in function of several experimental factors, such as morphology, choice of cations, metals and halide elements, mutual composition and preparation procedure.[64,65] In this scenario, it emerged that perovskites with mixed cations and halides are thermally and structurally more stable than the pure perovskite compounds: this observation opened a wide experimental and theoretical research activity, aiming at maximizing PSCs performance by choosing suitable elements, ions and functional groups. The resulting stability will be precious also for the commercial integration of PSCs with energy storage facilities.[66–75]

This Review focuses on one of the most promising and currently investigated element useful to further improve the strong characteristics and high performance of the PSC technology: caesium (Cs). It is the 45th most abundant element (the 36th among metals), more abundant than cadmium, tin and tungsten, mercury and silver. We will detail how Cs introduction in hybrid perovskites may improve the thermal stability at values exceeding 100 °C, optimize optical and electrical properties, alter the crystalline lattice to modulate the thermodynamic phase stability, precisely control the film formation, improve the device performance reproducibility, etc. Beyond Cs-doped hybrid perovskites, their fully inorganic counterparts, when the organic part is completely replaced by Cs cation, also show interesting aspects, further enriched by the introduction of Cs to improve the interface between the active material and the HTM/ETL components. Finally, some examples

[a] *Dr. F. Bella, Prof. Dr. C. Gerbaldi*
GAME Lab, Department of Applied Science and Technology (DISAT)
Politecnico di Torino, Corso Duca degli Abruzzi 24, 10129 Torino (Italy)
E-mail: federico.bella@polito.it
claudio.gerbaldi@polito.it

[b] *Dr. P. Renzi*
Dipartimento di Chimica, Università degli Studi "La Sapienza"
P.le A. Moro 5, 00185 Rome (Italy)
E-mail: polyssena.renzi@uniroma1.it

[c] *Dr. C. Cavallo*
Department of Physics (Condensed Matter Physics)
Chalmers University of Technology
Chalmersplatsen 1, 41296 Gothenburg (Sweden)
E-mail: carmen.cavallo@chalmers.se

The ORCID number(s) for the author(s) of this article can be found under: https://doi.org/10.1002/chem.201801096.

Part of a Special Issue to commemorate young and emerging scientists. To view the complete issue, visit Issue 47.

will be shown to demonstrate that Cs-based perovskites can be also applied in different fields apart from photovoltaics, such as photoluminescence probes, photodetectors, etc.

Caesium-Doping in Hybrid Perovskites

First reported by the group of Miyasaka, the application of perovskites to photovoltaic devices dates back to 2009.[76] Since then, an increasing interest towards this material has occurred, considering that perovskites as light absorbers exhibit broad absorption spectra, large extinction coefficient and high carrier mobility.[6,77,78] A continuous step forward has dominated the last years; however, improvements of PCE and stability are still needed for a future large-scale production. In the PSCs field, hybrid organic–inorganic materials can be divided into three main groups accordingly to their composition:

1) three-dimensional (3D) perovskites with the general formula ABX_3 (Figure 1 A);[1,2,76,77,79–82]
2) two-dimensional (2D) perovskites with the general formula A_2MX_4, characterized by organic ammonium layers alternately stacked with inorganic layers (Figure 1 B);
3) quasi-2D perovskites $A_2C_{m-1}B_mX_{3m+1}$ ($C{=}CH_3NH_3^+$; $m{=}$ number of inorganic monolayer) in which the multi-layered perovskite sheets are sandwiched between the organic ammonium layers (Figure 1 C).[83]

Considering that different degradation pathways, such as thermal decomposition,[84–86] light-induced trap-state formation,[87] phase transition[88,89] and bias-induced ion migration,[90] affect the device operation, this section will focus on Cs-doping as strategy to solve these drawbacks.

Among 3D materials, the methylammonium lead halide perovskites ($MAPbX_3$) are the most extensively applied, despite their instability due to structural phase transition at 55 °C[88] and thermal degradation at temperatures above 85 °C. To solve these issues, in 2014 Choi et al. started to investigate the effect

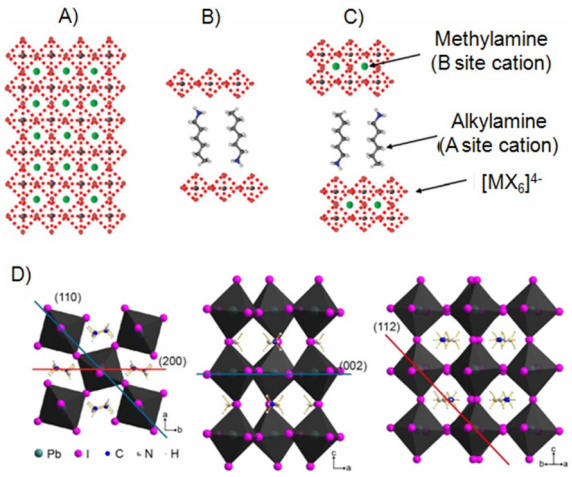

Figure 1. The crystalline structures of A) 2D and B, C) 3D perovskites; D) Schematic illustrations of (110), (002), (112) and (200) crystal planes from a perpendicular view, for perovskites composed of $(MAPbI_3)_{1-x}(CsPbBr_3)_x$ with x ranging from 0 to 0.2. Adapted and reprinted with permission.[97,116]

Federico Bella is Assistant Professor of Chemistry at Politecnico di Torino, Italy. He received both the BSc and MSc in Industrial Chemistry at University of Turin and the PhD in Electronic Devices at the Italian Institute of Technology. He has been visiting scientist at Universitat Politècnica de València, National University of Malaysia and École Polytechnique Fédérale de Lausanne. Currently, he is working in the field of solar cells and rechargeable batteries stabilization and optimization through polymeric and chemometric approaches. He is the winner of several prestigious awards and was a finalist for the European Young Chemist Award at the 6th EuCheMS Chemistry Congress. He has authored 65 publications and is also the Coordinator of the Young Group of the Italian Chemical Society.

Polyssena Renzi completed her PhD in 2014 at Sapienza University of Rome (Italy) under the supervision of Prof. M. Bella, working on the development of novel strategies for asymmetric synthesis. In 2015, she joined the group of Prof. R. M. Gschwind (Regensburg University, Germany) as a postdoctoral fellow, where she dealt with mechanistic investigations of organocatalyzed reactions by means of NMR techniques. In late 2017, she joined Sapienza University of Rome (Italy) as a postdoctoral researcher.

Carmen Cavallo is a postdoctoral researcher fellow at Chalmers University of Technology, Sweden, and a visiting scientist at the Commonwealth Scientific and Industrial Research Organisation (CSIRO), Australia. Currently, she is investigating new graphene-based materials in energy generation and storage applications. Carmen did her PhD in 2015 at the University of Rome "La Sapienza", Italy, where she was exploring the solar cells field (dye-sensitized and perovskite solar cells). She started her researcher career as a postdoctoral fellow in Sapienza University, Rome, supported by an intense collaboration with Stanford University (USA).

Claudio Gerbaldi, PhD in Material Science and Technology (2006), is Associate Professor of Fundamentals of Chemical Technology at the Politecnico di Torino. He is the leader of the Group for Applied Materials and Electrochemistry (GAME Lab) at the Department of Applied Science and Technology. He has a >15-years experience on electrochemical energy storage and conversion devices. He has 4 international patents and around 117 high-impact peer-reviewed scientific research articles. Among others, he has received the Piontelli Award for outstanding results in Electrochemistry from the President of the Italian Republic (2015) and the "UniCredit Award" for the Young Innovation in Research (2007).

of Cs-doping by replacing the organic cation in the $MAPbI_3$ structure with an inorganic cation.[91] The choice of Cs relied on its size, having a smaller radius than the MA counterpart. It can easily replace MA in the octahedral unit cell without affecting the crystal structure and the basic electronic properties of $MAPbI_3$ such as the low band gap of 1.5 eV. In this framework, Choi et al. reported the synthesis of $Cs_xMA_{1-x}PbI_3$ perovskites studying the influence of different amounts of Cs to improve the performances of inverted-type perovskite/fullerene planar heterojunction hybrid solar cells (ITO/PEDOT:PSS/perovskite/PCBM/Al; PEDOT:PSS = poly(3,4-ethylenedioxythiophene) polystyrene sulfonate; PCBM = phenyl-C61-butyric acid methyl ester). They observed that it was possible to tune the optical band-gap by changing the amount of Cs. Starting with a device with a PCE of 5.51% in the presence of pure $MAPbI_3$, it was possible to increase the PCE up to 7.68% by just adding 10% of Cs in the structure ($Cs_{0.1}MA_{0.9}PbI_3$). Amounts of Cs higher than 10% led to a reduction of the efficiency because of band-gap widening. Although the increased efficiency, the device was unstable under ambient conditions because the PEDOT:PSS is acidic in nature and the Al electrode employed is readily oxidized. The Cs-doping allowed for a better light absorption and morphology as well as for an increase in the energy difference between the perovskite valence bond and PCBM lowest unoccupied molecular orbital (LUMO) level, short-circuit current density (J_{sc}) and open-circuit voltage (V_{oc}).

The morphology of the film and its orientation are also very important factors to control to obtain a material with high performances. It is reported that $MAPbI_{3-x}Cl_x$ preferentially grows along the <110> and/or <002> directions during the crystallization process (Figure 1D).[92–94] However, by density functional theory (DFT) calculations, it has been predicted that orienting the film along the directions <112> and <200>, with these planes being characterized by a lower surface free energy, could be beneficial in terms of charge transfer improvement (Figure 1D).[94–96]

The preparation of films with a controlled orientation was reported for the first time in 2016 by Niu et al.[97] for a $(MAPbI_3)_{1-x}(CsPbBr_3)_x$ perovskite. During the spin coating, the progressive evaporation of the solvent in which all the precursors were dissolved, promoted the precipitation of CsI and PbI_2, which then acted as nucleation sites to allow a selective growth of the film along the desired <112>/<200> planes. A layer of heavily Cs-doped perovskite had the tendency to deposit on the bottom of the film. All these features promoted a gradual decrease on the J_{sc} values, an increase of both V_{oc} and fill factor (FF), while increasing the doping content. A PCE of 17.6% together with the enhancement of UV light stability was obtained with 10% of doping.

A systematic study of the thermal stability of $MAPbI_3$ and $Cs_xMA_{1-x}PbI_3$ film was reported by Niu et al.[98] The films were obtained from the one-step spin-coating method. Considering that a discrepancy was observed between the amount of Cs incorporated in the film and the amount of CsI employed in the precursors solution, X-ray photoelectron spectroscopy (XPS) was used to quantify the real amount of Cs incorporated in the film. The study revealed that the film decomposition was accelerated by the presence of oxygen in air that causes the oxidation of MA. The presence of a small amount of Cs could increase not only the device performance, but also its thermal stability. The thermal stability was evaluated by determination of the relative absorption at 700 nm after heating at 120 °C for 3 h (Figure 2A, B). A better stability was achieved in the presence of 9% of Cs with respect to the MA, but when its amount was higher than 23%, the absorption at 700 nm decreased, probably due to segregation phenomena. Indeed, oxidation phenomena and loss of A^+ cations were lowered by the partial replacement of MA by Cs^+ cations, thus a better stability, as well as pits- and pinholes-free film were obtained. Solar cell devices were assembled employing $Cs_{0.09}MA_{0.91}PbI_3$ and the stability evaluated at 85 °C in air without encapsulation by measuring current density/voltage (*J-V*) curves. $Cs_{0.09}MA_{0.91}PbI_3$ showed a final PCE of 18.1%. Around 80% of the initial PCE value was maintained with 9% of Cs-doping after an aging test, whereas in the absence of Cs, the per-

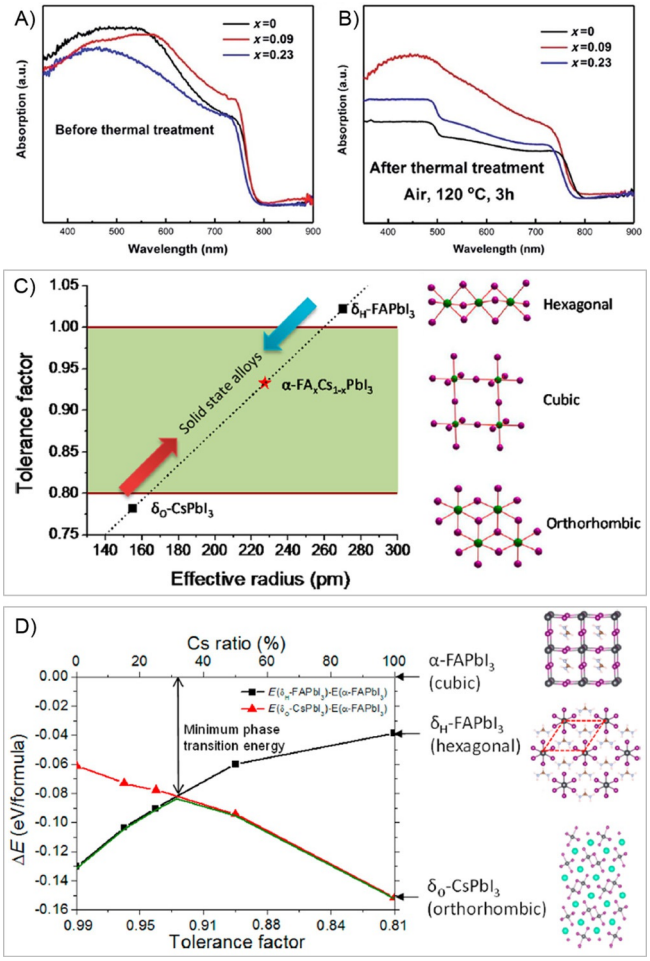

Figure 2. Thermal stability study of perovskite films with different Cs content: A) Perovskite films with compositions of $Cs_xMA_{1-x}PbI_3$ before thermal treatment, in which *x* represents the content in Cs; B) Perovskite films after thermal treatment at 120 °C for 3 h in air; C) Correlations between tolerance factor and crystal structure of perovskite materials; D) Calculated energy difference between α phase and different δ phases for $FA_{1-x}Cs_xPbI_3$ alloys with different Cs ratios. Adapted and reprinted with permission.[98,105]

formance was drastically reduced to the 40% of the initial value.

As an alternative to MA, FA cations can be employed as the A site in the 3D perovskites ABX_3. This leads to the formation of a material ($FAPbI_3$)[99,100] with a band gap of about 1.45 eV,[88,101] which is closer to the ideal value of 1.2–1.3 eV obtained for single-junction solar cells.[102] The main concerns about the employment of $FAPbI_3$ is its existence at room temperature in two polymorphs having different properties, which makes only one of the two phases suitable for photovoltaic applications.[89]

In general, the Goldschmidt tolerance factor (*t*), an empirical index calculated from the ionic radius of atoms, is employed to predict the crystal structure stability of the perovskite.[103] Good photovoltaic properties are obtained in the presence of a cubic structure, which is associated with a *t* value between 0.8 and 1. Values of *t* above 0.8 correspond to the formation of the hexagonal structure, whereas when the *t* value is lower than 0.8, the structure is preferentially orthorhombic.[103] For $FAPbI_3$, good photovoltaic properties are obtained in the presence of a cubic crystal structure, being characteristic of the α (or black) phase (Figure 2C). On the contrary, the most stable hexagonal crystal structure gives rise to the δ_H (or yellow) phase, which is characterized by a lower light absorption and not suitable for photovoltaic applications.[88,101,104] The transition between the two phases is possible but only at relatively high temperatures (165 °C). Interestingly, the stabilization of the α phase can be observed applying a protocol developed by Li et al., which is based on the combinations of materials having different *t* values, such as $FAPbI_3$ in the δ_H phase and $CsPbI_3$ in the orthorhombic δ_O phase (Figure 2D).[105]

With a Cs-doping level of 15%, alloying is responsible for the reduction of the transition temperature to 125 °C, the stabilization of the α phase and the suppression of the decomposition to PbI_2. Moreover, this material showed increased stability to humidity, as demonstrated by the absence of changes in the UV/Vis spectra above 400 nm of $FA_{0.85}Cs_{0.15}PbI_3$ after storage at a constant humidity of 15% for 10 to 18 days, whereas the pristine $FAPbI_3$ decomposed rapidly to PbI_2. The article from Li et al. demonstrated that the δ→α phase transformation is a crucial step in the solution-growth process of $FAPbI_3$ perovskite thin films.[105]

In $FAPbI_3$, the δ phase is formed during the film production and its conversion to the α phase requires a thermal treatment that likely causes degradation if performed at too high temperature. Spray reaction is used to circumvent the phase separation during solvent evaporation, thus obtaining films with a pure α phase structure. In this case, the solvent is converted to vapour before contacting the TiO_2 surface. Xia et al. applied the spray reaction to prepare films of $FA_{1-x}Cs_xPbI_3$ with different amounts of Cs.[106] A solution of CsI and PbI_2 in dimethylformamide (DMF) was prepared and applied by spin-coating on the TiO_2 film. Successively, formamidinium iodide (FAI) was dissolved in isopropanol and sprayed at 160 °C on top of the previously formed layer, thus releasing the perovskite $FA_{1-x}Cs_xPbI_3$. After washing with isopropanol, the material was annealed. By this method, films in the α phase with high quality were obtained with up to the 30% of Cs-incorporation. According to its content, Cs could modulate the band-gap and the absorption intensity of $FA_{1-x}Cs_xPbI_3$. Interestingly this spray method led to devices with stabilized PCE values also in the absence of Cs, but with different transient times. In the presence of Cs, a stabilized value of PCE was obtained much faster (3.4 s for $FA_{0.9}Cs_{0.1}PbI_3$ vs. 8.5 s for $FAPbI_3$), implying that the incorporation of Cs ions accelerated the achievement of the device equilibrium state. The stability of the unsealed device against humidity was also studied by aging test at 50% relative humidity (RH) and 20 °C for 100 h. Remarkably, the incorporation of 10% Cs ions stabilized the device, which maintained its dark colour also after aging, whereas the $FAPbI_3$-based device turned yellow. PCE value of 14.2% was obtained for $FA_{0.9}Cs_{0.1}PbI_3$. The previous value decreased to 12.5% after aging.

Subsequently, it was shown that also the grain size of the non-perovskite δ phase doped with small amounts of Cs is important to obtain high-quality α-$FAPbI_3$(Cs) films without voids at the interfaces. A uniform thin film can be prepared by employing the one-step extraction-based antisolvent-solvent method.[107] A precursor solution was prepared in dimethyl sulfoxide (DMSO) or DMF. Then, during crystallization of the solution, the solvent was extracted and the film formed as yellow non-perovskite δ phase independently from the type of solvent used. A thermal annealing at 150 °C was performed, which induced both δ→α transition and grain coarsening. Despite the grains were about 7 times larger in DMF than in DMSO, the coarsening proceeded much faster in DMF, thus leading to the formation of defects at the α-$FAPbI_3$(Cs)/substrate interface, as shown in Figure 3A–D. Grain coarsening was negligible in DMSO, leading to the formation of stable thin films lacking defects, thus the material was more stable and efficient under ambient atmosphere. Besides the introduction of Cs, also a co-doping meant to replace or substitute the halogen atoms in the X position of a 3D perovskite can be useful to enhance the properties of the material for photovoltaic application. In this context, Chiang et al. reported about the introduction of the SCN^- pseudohalide in the X site of mixed FA/Cs organic-inorganic hybrid perovskite.[108] Keeping constant at 9:1 the ratio of FA:Cs, the doping level of SCN^- anions was modulated in the range 0–10% with respect to the content of iodine ions in the precursors solution to obtain a perovskite with the general formula $FA_{0.9}Cs_{0.1}Pb(SCN)_yI_{3-y}$. The addition of SCN^- ions was shown to have beneficial effects over the quality of the film (Figure 3F,G). However, its amount had to be kept below a certain value; indeed, the increase of SCN content was likely associated to the decrease in the absorbance. A slower nucleation rate was also associated with larger grain size. The optimal doping was obtained at 3.75% of $Pb(SCN)_2$ in $FA_{0.9}Cs_{0.1}PbI_3$, which resulted in a PCE of 16.9%. J_{sc} and FF dropped at 10% doping level. It was observed that the content of S on the surface was lower with respect to the one added in the precursor solution, likely ascribable to the evaporation of SCN^- ions during annealing or the incorporation of SCN^- ions into the PbX_6^{4-} octahedral, thus resulting in enhanced crystal stability. As shown in Figure 3F,G, the SCN-

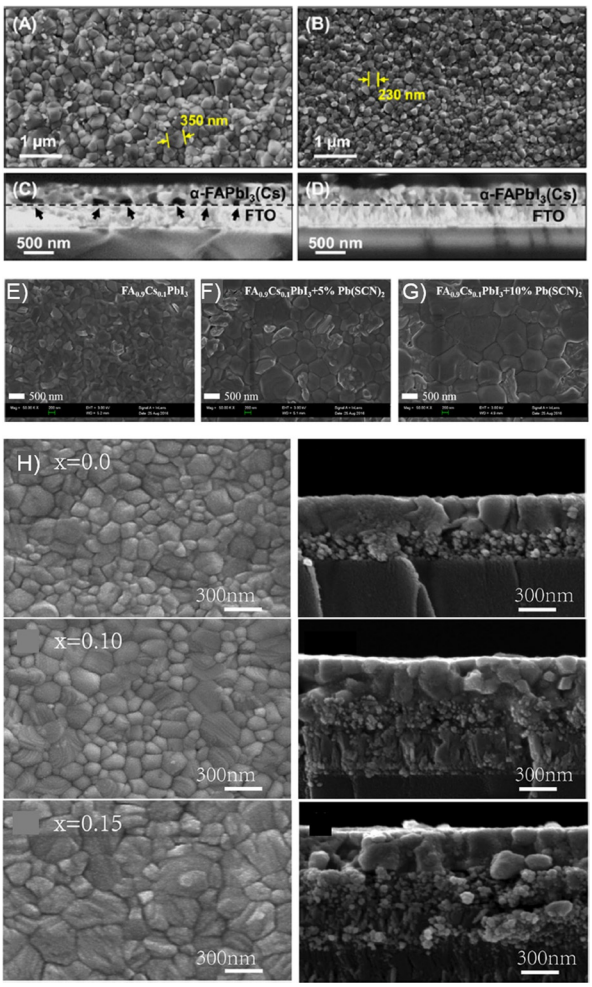

Figure 3. A–B) Top-view and C-D) Cross-sectional SEM images of the "black" α-$FAPbI_3$(Cs) hybrid organic-inorganic perovskite thin films processed using DMF (panels A and C) and DMSO (panels B and D) as the solvents in the precursor solutions. Scanning electron microscope (SEM) images of one-step spin-coated $FA_{0.9}Cs_{0.1}PbI_3$ with E) 0, F) 5 and G) 10% $Pb(SCN)_2$ doping. H) Top view (left column) and cross-sectional (right column) SEM images of perovskite films with different CsBr doping levels. Adapted and reprinted with permission.[107–109]

doping allowed obtaining grains with large-size and high crystallinity, which were associated also with longer carrier lifetime and increased moisture stability with respect to the conventional $MAPbX_3$ perovskite.

Co-doping with both Br^- and Cs^+ ions is another way to improve both the stability and the efficiency of perovskites. These ions can be introduced into the $CH_3NH_3PbI_3$ perovskite as CsBr to form triple cation materials.[109] As shown by X-ray diffraction (XRD), Br^- tends to replace the I^- ions linked to the Pb^{2+} ones inducing modifications in the morphology of the perovskite film. Br^- allows the growth of larger grains with a consequent enhancement of optical absorption: the grain size increased from 42.5 to 63.5 nm in the absence of doping and upon addition of 10% of CsBr, respectively. The larger grain size indicates a smaller area occupied by grain boundaries, which results in fewer interface defects to induce the recombination of photogenerated carriers (Figure 3H). Moreover, an increase in V_{oc} was also observed. In fact, after doping, the perovskite band-gap was blue-shifted accordingly to the broadening of the band-gap of plain thin films after the addition of Cs^+ or Br^- ions.[110–112] The perovskite with 0.9:1:0.1 ratio of CH_3NH_3I:PbI_2:CsBr showed a PCE of 13.6%, which is much higher than the 9.8% value without doping.

A step forward in the development of perovskite materials is represented by the introduction of a third cation in MA/FA compounds. Actually, small amounts of Cs are beneficial to the suppression of those impurities in the crystalline phase that make the performances of MA/FA perovskites not reproducible. Interestingly, the Cs^+ cation is incorporated into the perovskite lattice and, having a smaller radius than FA and MA, is able to reduce the *t* value and drive the crystal towards a cubic structure, matching the black phase that is optimal for photovoltaic applications.[113] The formation of the hexagonal yellow phase is suppressed, not being stabilized anymore at room temperature. Triple cation perovskites having the formula $Cs_x(MA_{0.17}FA_{0.83})_{(100-x)}Pb(I_{0.83}Br_{0.17})_3$ also showed improved thermal stability. No bleaching or limited bleaching was obtained after storage at 130 °C for 3 h in dry conditions, whereas the pristine sample turned yellow. Very high efficiency of 21.1% was obtained with an output at 18% under operational conditions after 250 h with 5% of Cs-doping (Figure 4B). These triple cation perovskites revealed to be robust and showed reproducible performances also in the case of experimental variability during fabrication (Figure 4A).

XPS was used to probe the triple cation-based PSCs and to find their composition versus performances correlation.[114] The highest FF was achieved with 5% of Cs content, which was able to maintain the stoichiometric ratios of I:N, Br:Pb and I:Pb inside the $(MA_{0.15}FA_{0.85})Pb(I_{0.85}Br_{0.15})_3$ lattice. Moreover, the electrostatic interactions between the Cs^+ cation and the I^-/Br^- anions helped to stabilize the crystalline lattice. When added in low quantities (5%), Cs^+ could arrange itself in the depth of the light-absorber layer, in fact—also after Ar-sputtering—Pb^{2+} was retained and the valence band level was the least perturbed.

Salado et al. reported on a kinetic study about triple cation-based PSCs to elucidate the role of the Cs^+ cation[115] by means of scanning probe microscopy (SPM) and electrochemical impedance spectroscopy (EIS) experiments. The best performing device contained 5% of Cs, resulting in $Cs_{0.05}(MA_{0.15}FA_{0.85})_{0.95}Pb(I_{0.85}Br_{0.15})_3$, and a fixed 90 mM concentration of the HTM $N^2,N^2,N^{2'},N^{2'},N^7,N^7,N^{7'},N^{7'}$-octakis(4-methoxyphenyl)-9,9′-spirobi[9H-fluorene]-2,2′,7,7′-tetramine (Spiro-OMeTAD). PCE was 17.53%. Upon illumination and under short-circuit, the accumulation of charges was observed at grain boundaries. The migration of MA cations was reduced through stabilization of the crystal structure by FA and hydrogen bond formation with the Pb octahedral site. Moreover, Cs^+ was able to build up strong electrostatic attractions with halide ions, thus stabilizing the lattice.[114] The average current carrying ability of the mixed-perovskite was enhanced and a delocalized distribution of charges was observed across the surface in the presence of Spiro-OMeTAD. In mixed halide perovskites, the incorporation of Cs reduced the recombination resistance and increased the electron lifetime.

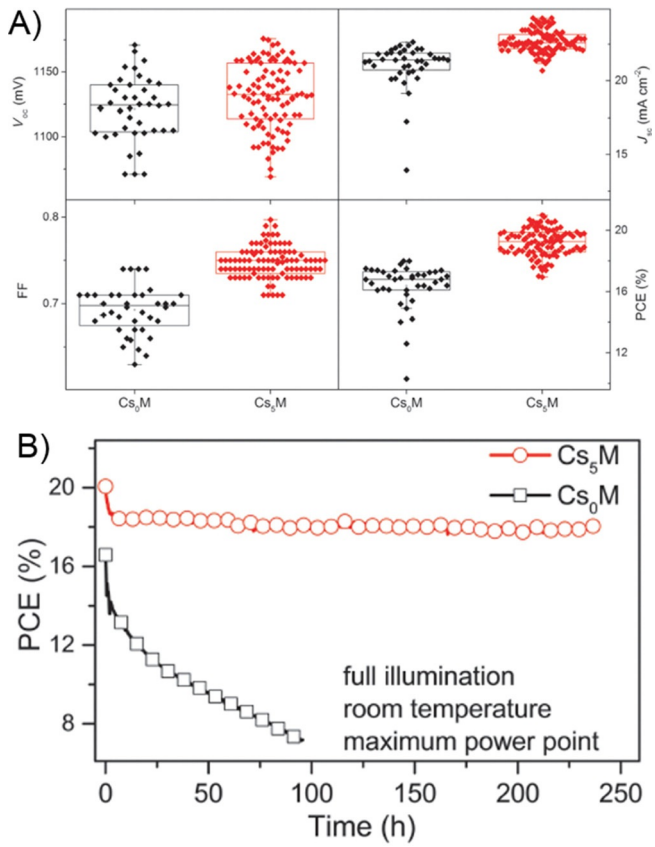

Figure 4. A) Statistics of 40 controls (Cs_0M) and 98 Cs-based (Cs_5M) devices as collected over 18 different batches. All device parameters as well as the standard deviation improved, and 20 independent devices showed efficiencies >20%. B) Aging for 250 h of high performing Cs_5M and Cs_0M devices under N_2 atmosphere held at room temperature under constant illumination and maximum power point tracking. The maximum power point (MPP) was updated every 60 s by measuring the current response to a small perturbation in potential, and a *J-V* scan was taken periodically to extract the device parameters. Adapted and reprinted with permission.[113]

The synthesis of quasi-2D perovskites was reported by Hamaguchi et al. in 2017 by reacting the organoamine halide acid salt *n*-$C_6H_{13}NH_3I$ and methylammonium iodide (MAI) or FAI or CsI with PbI_2 in stoichiometric amounts employing DMSO or DMF as solvents according to the stability of the precursors.[116] The quasi-2D perovskite is characterized by the introduction in the crystalline structure of MA, FA or Cs in the B site cation position. The material has the general formula (*n*-$C_6H_{13}NH_3)_2$(B)Pb_2I_7, in which B can be MA, FA or Cs. The crystalline orientation can be controlled by the pre-heating temperature and rotational speed during spin coating. (*n*-$C_6H_{13}NH_3)_2$(FA)Pb_2I_7 with perpendicular partially crystalline growth showed better photovoltaic properties in mesoscopic PSC application than (*n*-$C_6H_{13}NH_3)_2$(MA)Pb_2I_7 and (*n*-$C_6H_{13}NH_3)_2$(Cs)Pb_2I_7. However, these quasi-2D perovskites showed lower performances compared to 3D PSCs due to the lack of light absorption in the range 550–600 nm.

Humidity is one of the most relevant factors affecting the stability of perovskites.[117,118] A study about moisture stability of Cs- and Br-containing mixed perovskites was reported by Li et al.[119] Despite showing better resistance to moisture, after exposure at 70% RH the perovskite underwent a rapid degradation with the formation of the yellow $CsPbI_3$ phase probably due to the absorption of water on the film surface, followed by infiltration of moisture between the grain boundaries. However, the erosion phenomena could be suppressed by the introduction of phenylethylammonium iodide (PEAI) passivation layer. This layer not only helped in retarding the degradation, but enhanced the PCE values. Perovskite $FA_{0.8}Cs_{0.2}PbI_{2.7}Br_{0.3}$ was chosen to test the applicability of the passivation layer. Figure 5A,B shows the change in the film morphology after aging at 70% RH in the dark. After 6 h, the film started to be extensively compromised because of degradation processes due to the formation of $CsPbI_3$, as confirmed by its absorption peak at about 420 nm. In addition, other degradation products were formed. The material did not suffer from the same degradation when exposed to 25% RH for 10 days (Figure 5A).

The highest PCE of 13.7% for 2D organic-inorganic perovskites was reported in 2017 by Zhang et al., by doping 2D $(BA)_2(MA)_3Pb_4I_{13}$ perovskite materials with 5% of Cs^+ cations.[120] Doping was again beneficial to obtain an increment of grain size, a controlled crystal orientation, a reduction of trap-state density, surfaces with better quality and a superior charge-carrier mobility. In the presence of high humidity, the device demonstrated enhanced operation, with a degradation of only 10% obtained at 5% Cs doping after exposition under 30% RH for 1400 h (Figure 5C). For the first time, 2D materials showed stability not only under humidity, but also under heating. Films of high quality were grown by the hot-casting method developed by Tsai et al.[121] with DMSO as solvent, which was able to work as ligand for the PbI_2 precursor, thus driving the crystallization process. Moreover, the Cs^+ cation could slow down the process helping the 2D grains to grow larger. The films resulted more shining when the perovskite was doped with 5% of Cs, suggesting a smoother surface, the homogeneity of the film and the likely higher specular reflection. The surface got distorted with higher amount of Cs (15%). Several humidity tests revealed that the 2D perovskites were more tolerant towards humidity and superior properties were obtained by Cs-doping (Figure 5D).

A strong resistance towards humidity was obtained by the introduction of *n-butyl*ammonium (BA) cations into a mixed CsFA lead halide perovskite.[122] By employing 3% of BA with respect to FA/Cs, the increase of grain size was combined with the formation of 2D platelets arranged between the 3D perovskite grains. BA^+ ion had larger radius than Cs^+ and FA^+ ones, which caused modification in the lattice constants. The junction between the 2D and 3D phases was assumed to be characterized by a clean electronic interface; in this way, when the charges arrived at the interface they were reflected and kept by the 3D perovskite, eliminating the problem of charge recombination that was observed in the presence of grain boundaries.[123] The presence of BA enhanced the crystallinity and reduced the hysteresis in *J-V* plots. The resulting device was definitely stable; indeed, the solar cell could be assembled in air, which accounts for its promising prospects in long-term outdoor applications. Remarkably, PCE was 19.5% and the

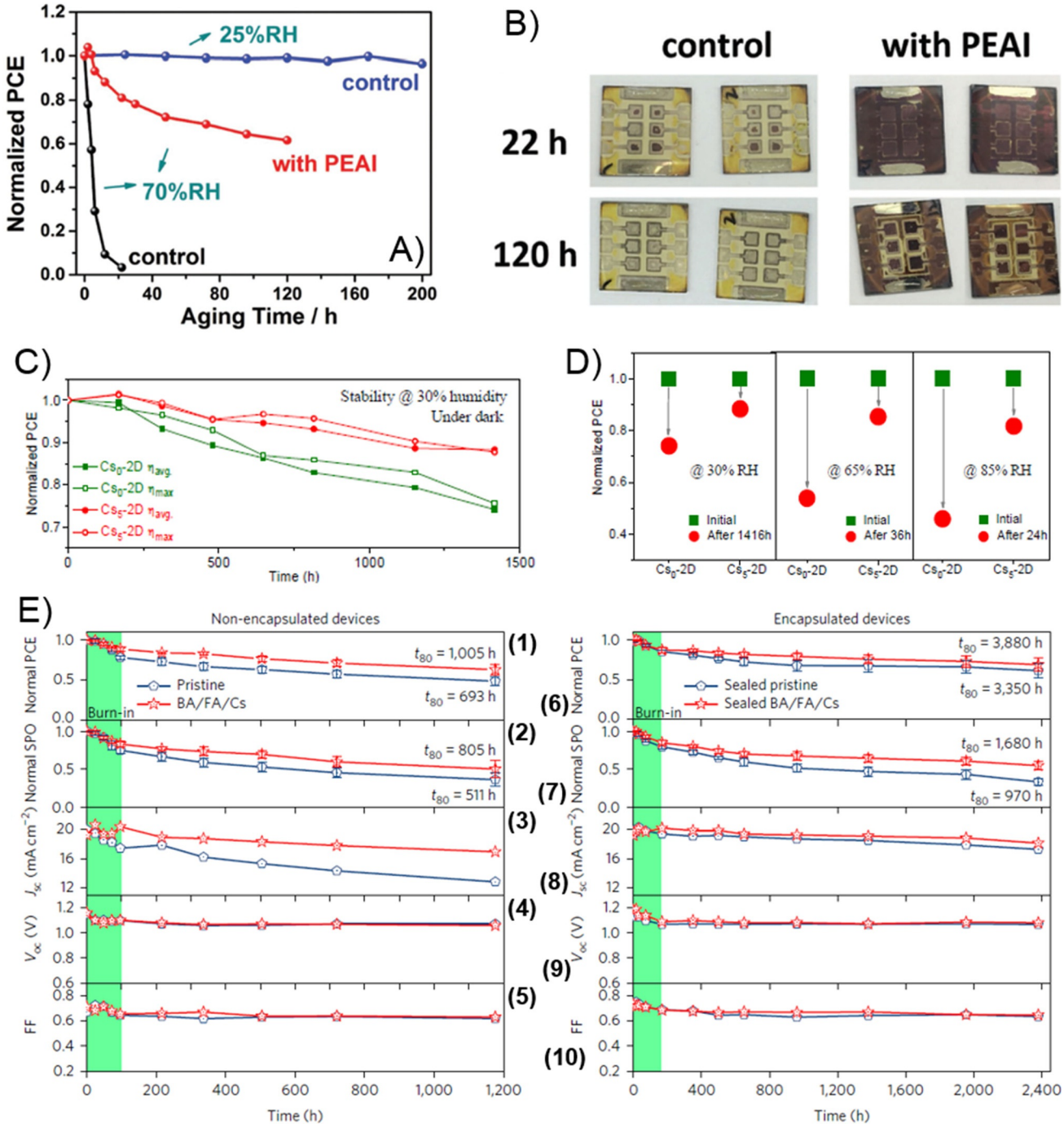

Figure 5. A) Moisture stability test of inverted devices without PEAI treatment, and B) Images of aged devices in the 70% RH dark condition. Stability measurements for the Cs_0-2D and Cs_5-2D PSCs; C) Long-term stability measurements of both solar cells without any encapsulation under ambient condition, viz. 30% RH; D) Humidity tolerance measurements for both solar cells at different humidity: 30, 65 and 85% RH. E) Comparison of stability of high-performing non-encapsulated (**1**–**5**) and encapsulated (**6**–**10**) solar cells using $FA_{0.83}Cs_{0.17}Pb(I_{0.6}Br_{0.4})_3$ (navy blue lines; labelled as pristine) and $BA_{0.09}(FA_{0.83}Cs_{0.17})_{0.91}Pb(I_{0.6}Br_{0.4})_3$ (red lines; labelled as BA/FA/Cs) perovskite active layers. Devices are aged under Xe-lamp simulated full-spectrum AM1.5, 76 mW cm^{-2} equivalent irradiance in air (45% RH) without any ultraviolet filter, held at open-circuit during ageing. Adapted and reprinted with permission.[119,120,122]

band-gap was 1.61 eV. Under simulated sunlight, about 80% of the efficiency was maintained after 1000 h of work in air (Figure 5E). The operational time could be extended to 4000 h upon device encapsulation. An additional enhancement of stability and performances is likely possible by proper optimisation of the 2D/3D phase heterostructures engineering.

Enhanced resistance to humidity was observed by the partial replacement of Pb with Sn, which is also highly desired in the light of a future commercialization of Pb-free PSCs. Sn was chosen as possible candidate having a similar radius to Pb.[124] However, the formation of high quality films for these binary Sn-Pb perovskites, which have band-gaps around 1.2–

1.3 eV,[125] was much more difficult because of the fast crystallization between SnI_2 and MAI,[126] the easy oxidation of Sn^{2+} to Sn^{4+} and the formation of pinholes when the amount of Sn exceeded 25%.[127,128] Slowing down of the crystallization process was likely observed by substitution of MA and FA ions through Cs-doping.[129] Cs may reduce also the oxidation of Sn^{2+} (after storage at ambient temperature and RH 35±5%) and increase the stability at high temperatures and humidity. The highest PCE of 12.7% was obtained with 10% of Cs doping in the presence of 50% of Sn, that is, the highest percentage of Sn ever added in a perovskite material. Most important, the perovskite $MA_{0.9}Cs_{0.1}Pb_{0.5}Sn_{0.5}I_3$ maintained about 76% of the initial PCE after storage at ambient temperature for 20 days at RH of 35±5%.

For the practical application of perovskites, their synthesis should be controlled to get a well-defined morphology. The production of lead halide perovskites is generally based on the one-step and two-step protocols. In the first one, organic and Pb-salt precursors are dissolved and mixed together in a polar solvent at 70 °C and then spin-coated. In the second one, a layer of Pb-salt is firstly deposited as a thin film, which is then soaked in a solution containing the organic salt.[4,6,76,91,130–132] These approaches are generally characterized by the difficult control of the final film composition since the organic ammonium cations, being volatile, can evaporate during the annealing process. Alternative to the solution preparation, which is limited by the control of various parameters, Murugadoss et al. reported a large-scale fast powder production method.[133] In this process, lead halide perovskites were obtained by mixing a hot DMF solution (100 °C) of perovskite with chlorobenzene (1:1 ratio). After stirring for 1 min, the solution was dispersed into a Petri dish and heated at 120 °C on a hot mantle. Different crystal morphologies (such as nanorods, nanofibers, dense packed grains, nanowires and spherical nanoparticles) for $Cs_xMA_{1-x}PbI_3$ were accessed in a controlled way, accordingly to the amount of Cs added as black powder. As shown in Figure 6 A–D, low concentration of Cs resulted in the formation of little grains ($x=0.5$), similarly to what obtained by normal spin coating. More ordered structures, such as nanorods ($x=0.2$), nanowires ($x=0.4$) and nanofibres ($x=0.6$), were obtained by increasing the amount of Cs.

The first application of gas-phase-assisted mixed-cation compositional modulation was reported by Luo et al. $Cs_xFA_{1-x}PbI_3$ solar cells were produced in the stabilized α phase.[134] This method relayed on the preparation of a solution of the CsI and PbI_2 precursors in a dry solvent, which was spin coated on the support. Then, $Cs_xFA_{1-x}PbI_3$ was formed by the deposition of FAI vapour. Considering that the film was grown in the presence of a saturated atmosphere of FAI, the composition of the film could be carefully controlled by the Cs/Pb ratio in the precursors solution. The control over the morphology was obtained, but the amount of Cs had to be kept below 0.3 to avoid phase segregation. The optimal amount of 0.15 ($Cs_{0.15}FA_{0.85}PbI_3$) led to a PCE value of 14.45% and moisture resistance because about 88% of initial PCE was retained after one week of exposure to air.

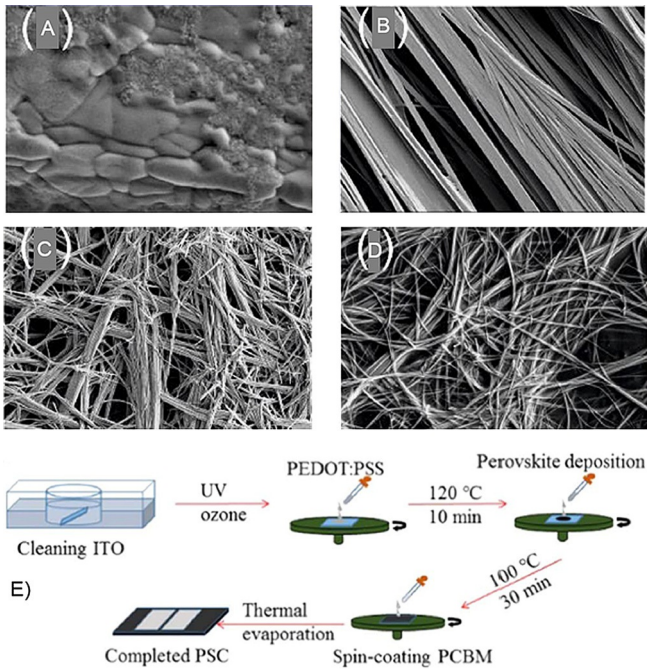

Figure 6. FESEM images of $Cs_xMA_{1-x}PbI_3$ perovskite powders having different morphologies obtained with different amounts of Cs: A) Tightly packed grains ($x=0.5$), B) Rod like structures ($x=2$), C) Nanowires ($x=4$), D) Nanofibers ($x=6$). E) Schematic representation of low-temperature two-step spin-coating protocol. Adapted and reprinted with permission.[133,135]

Finally, in the light of a future commercialization, Ye et al. managed to implement the formation of pinhole-free perovskite in flexible photovoltaic devices.[135] Mixed MA and FA perovskites were doped with CsI employing a low-temperature process based on a two-step spin coating. The device fabrication process is summarized in Figure 6 E. It allowed the production of high efficiency flexible photovoltaic devices. The doping in the mixed perovskite allowed obtaining a more compact film with an efficient charge carrier injection/transport within the device with only 5% of CsI. A doubled V_{oc} was obtained with respect to the control device (0.92 V with 5% CsI vs. 0.46 V for the control). PCE of 12.1 and 14.6% were reached in the flexible and rigid devices, respectively, starting from 8.9 and 11.3% without doping. Moreover, about 94% PCE was maintained after 400 bending cycles. A global overview of the overall efficiencies of Cs-doped hybrid organic-inorganic PSCs is given in Table 1.

Caesium-Doping in Inorganic Perovskites

After the first report in 2009,[76] hybrid perovskite absorbers[136] had been promised to revolutionize the research and development on dye-sensitized, organic, and thin film solar cells. However, the organic moiety in these compounds is extremely hygroscopic, volatile, and prone to thermal and thermodynamic decomposition.[137]

"Is the organic cation necessary to obtain high quality perovskite solar cells?" This is the question Kulbak et al. answered when they replaced the polar, organic molecules (MA/FA) with

Table 1. Summary of structures and PCE values obtained for Cs-doped hybrid organic-inorganic PSCs.

Perovskite	PCE [%]	Ref.
$Cs_5(MA_{0.17}FA_{0.83})_{95}Pb(I_{0.83}Br_{0.17})_3$	21.2	[113]
$BA_{0.09}(FA_{0.83}Cs_{0.17})_{0.91}Pb(I_{0.6}Br_{0.4})_3$	19.5	[122]
$Cs_{0.09}MA_{0.91}PbI_3$	18.1	[98]
$(MAPbI_3)_{0.9}(CsPbBr_3)_{0.1}$	17.6	[97]
$Cs_{0.05}(MA_{0.15}FA_{0.85})_{0.95}Pb(I_{0.85}Br_{0.15})_3$	17.53	[115]
$FA_{0.9}Cs_{0.1}Pb(SCN)_{0.375}I_{2.625}$	16.9	[108]
$Cs_{0.15}FA_{0.85}PbI_3$	14.45	[134]
$FA_{0.9}Cs_{0.1}PbI_3$	14.2	[106]
$(BA)_2(MA)_3Pb_4I_{13}$	13.7	[120]
$(CH_3NH_3I)_{0.9}(PbI_2)_1(CsBr)_{0.1}$	13.6	[109]
$MA_{0.9}Cs_{0.1}Pb_{0.5}Sn_{0.5}I_3$	12.7	[129]
$Cs_{0.1}MA_{0.9}PbI_3$	7.68	[91]

a more stable non-polar component (Cs^+) in an all-inorganic PSC.[138] Furthermore, the partial replacement of inorganic cations, such as Cs^+ and Rb^+, was shown to improve the mechanical and thermal stability of MA/FA halide perovskites.[139] By finely tuning the *t* value, we can predict the stability and/or the distortion of the crystal perovskite materials structure.[140] Mixing organic cations such as FA or MA with small amounts of Rb^+ or Cs^+ cations can lead to a more favourable *t* value, which facilitates the stabilization of the photoactive perovskite phase in a broad temperature range, resulting in stable devices.[141] Nowadays, all-inorganic perovskite (i.e., the organic component is completely replaced with a Cs^+ at the A-site of the crystal structure) is the ultimate solution to mitigate the problems of air-stability and chemical decomposition, together with matching the peculiar characteristics of PV materials and the efficiency performance of the hybrid organic–inorganic solar cells.[1]

Caesium metal halide perovskites ($CsBX_3$), isostructural to perovskite $CaTiO_3$ and related oxides, consist of a Cs-based cuboctahedral cavity at the centre of the corner-sharing lead/tin halide octahedral network.[142] The interaction of Cs^+ with the halide-dominated perovskite structure is potentially very different and understanding its effect on the perovskite structure is crucial to improve solar cell performances. First synthesised by Wells et al.,[143] the perovskite $CsPbI_3$ possesses an excellent combination of band-gap,[144,145] thermal stability, and absorption coefficient for photovoltaic applications,[146,147] if compared to the bromide ($CsPbBr_3$) and chloride ($CsPbCl_3$) counterparts. In general, materials with a *t* value of 0.9–1.0 have an ideal cubic structure. Unfortunately, the Cs^+ cation is too little to form a stable perovskite structure for $CsPbI_3$ at room temperature.[148] The desirable black phase (α-$CsPbI_3$, $Pm\bar{3}m$ cubic symmetry) is not stable above 320 °C in air with a *t* value of 0.81, which degrades rapidly to a non-perovskite yellow phase (γ-$CsPbI_3$, *Pnma* orthorhombic symmetry). When applied in a solar cell, γ-$CsPbI_3$ did not exceed 0.09% of PCE.[91] The stabilization of the polymorph α-$CsPbI_3$ at room temperature is one of the most though challenges to use such material in solar cells as well as in tandem devices.[149]

Opening the way to fully inorganic perovskite solar cells, Eperon et al. in 2015 showed that a bulk thin film of the yellow phase could be converted into the black phase at only 100 °C by adding a small amount of HI in the precursor solution (1:1 CsI:PbI_2 solution in DMF).[150] Upon crystallization, HI induced the formation of smaller grains, which are responsible for the stabilisation of the black phase at room temperature. Figure 7A,B shows the structure of both $CsPbI_3$ phases (γ, orthorhombic at room temperature, and α, cubic at $T > 300$ °C or 100 °C with HI), together with the absorbance spectra of black (band-gap of ≈1.73 eV) and yellow (2.82 eV) phases. As a result, the first example of $CsPbI_3$ working solar cell was obtained with preliminary PCE values of 1.7 and 2.9% for the inverted *p*-i-n and the regular n-i-p devices, respectively. The devices' architecture is shown in Figure 7C. However, the ambient instability problem remained; indeed, this study only reported a solution route to form the black $CsPbI_3$ perovskites thin film at room temperature in a totally air-free environment.

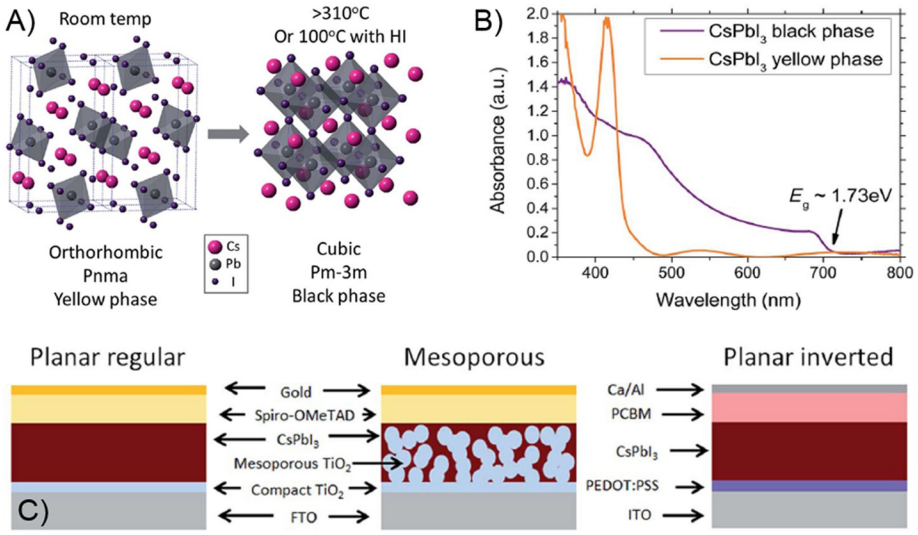

Figure 7. A) Structural scheme of $CsPbI_3$ phases and B) Absorbance spectra of black and yellow phases of $CsPbI_3$ thin films; C) Architecture of the solar cell device. Adapted and reprinted with permission.[150]

Luo et al. developed this method further in an open-air condition (with RH below 30% at room temperature) by a sequential isopropanol treatment process. The material demonstrated an enhanced efficiency of 4.13%.[151]

Based on these results, Hu et al. hypothesized that partially substituting Pb^{2+} (1.19 Å) with a smaller cation like Bi^{3+} (1.03 Å) would further stabilize the α-$CsPbI_3$ phase at room temperature.[152] The *t* value increased from 0.81 (α-$CsPbI_3$) to 0.84 (α-$CsPb_{1-x}Bi_xI_3$). They used Snaith's one-step deposition method,[150,151] by employing precursor solutions (PbI_2 and BiI_3) to obtain a Bi-incorporated compound ($CsPb_{0.96}Bi_{0.04}I_3$). The role of Bi^{3+} is quite similar to HI and, with an optimal amount of 4 mol%, the α-phase was found to be stable for more than 6 days. The possible mechanism for the stabilization of α-$CsPbI_3$ by the addition of HI or Bi^{3+} is shown in Figure 8. The $CsPb_{0.96}Bi_{0.04}I_3$-based thin film device exceeded 13% of PCE and maintained 68% of this value after 168 h. In all these synthetic procedures, only DMSO and DMF were used to sufficiently solvate Cs and Pb halide precursor salts.

Ramadan et al. tried to optimise the thin film fabrication process by studying the effects of solvent selection on the electronic, structural and morphological properties of $CsPbI_3$ thin films and compared solvent mixtures to additive solutions.[153] Thin films of $CsPbI_3$ were fabricated via spin-coating on fluorine-doped tin oxide (FTO) glass from 0.5 M solutions, using DMF, DMSO, DMF with 3.3% HI, and a 2:1 DMF:DMSO mixture as solvents. In this study, the authors demonstrated the relationship between the processing of the solvent and the interfaces of the films, even if it was not possible to select a proper solvent for the process.

Besides the commonly reported cubic perovskite (α-$CsPbI_3$) and non-perovskite (γ-$CsPbI_3$) phases, α-$CsPbI_3$ might also transform into an uncommon orthorhombic perovskite structure (β-$CsPbI_3$) via distortion of PbI_6 octahedra without breaking the 3D Pb-I network. Unfortunately, the conversion to the yellow phase is very rapid and identifying the single-crystal structure of β-$CsPbI_3$ is still now an open discussion. Using time-resolved photoluminescence quenching experiments, Fu et al. estimated for the first time that the electron and hole diffusion lengths in the orthorhombic (β-$CsPbI_3$) perovskite phase with surface ligands (oleylammonium (OA) or phenylethylammonium (PEA)) acetate could be up to 350 and 94 nm, respectively, indicating efficient charge transport within the film.[154] Excellent room temperature phase stability of the films, enabled by surface functionalization, together with their good photophysical properties were reported. A proof-of-concept planar heterojunction solar cell based on stabilized $CsPbI_3$ perovskite thin film demonstrated a PCE of about 6.5%.

It is known that colloidal nanocrystals of $CsPbI_3$ (typically, in the 2–20 nm range) are more stable in the cubic phase at room temperature than in bulk $CsPbI_3$, unlike polycrystalline thin films, in which the phase transition is expected to be simi-

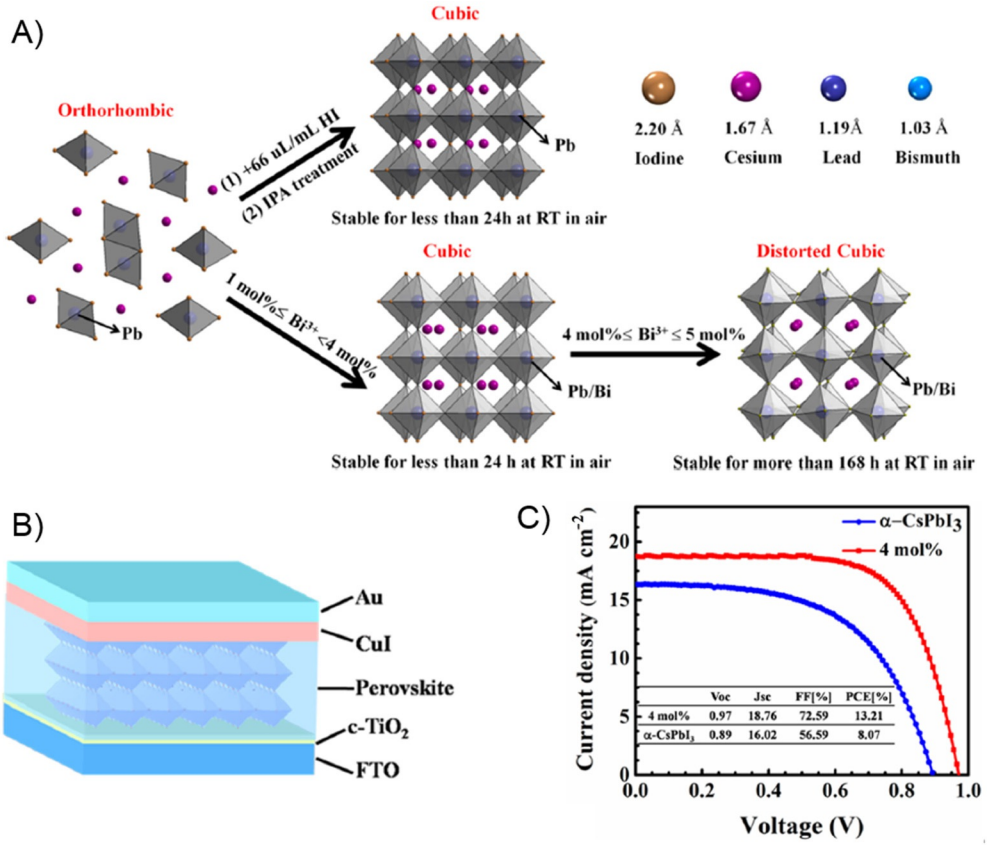

Figure 8. A) Possible mechanisms for stabilization of α-$CsPbI_3$ by adding HI or Bi^{3+} in the precursor solution; B) Illustration of the fully inorganic PSC; C) *J-V* characteristics of the best cells based on the controlled α-$CsPbI_3$ and $CsPb_{0.96}Bi_{0.04}I_3$. Adapted and reprinted with permission.[152]

lar as in the bulk.[155] Moreover, the possibility to confine these perovskites at the nanoscale paves the way to synthesise band-gap tuneable $CsPbI_3$ perovskites.[156] Easily processed in solution (e.g., by means of simple spin-coating), colloidal nanocrystals of inorganic lead halide perovskite could be dispersed into a variety of solvents and matrices and, eventually, incorporated into various device.[157] Also known as nanocrystal quantum dots, colloidal nanocrystals are being intensively studied as future optoelectronic materials.[158,159]

Protesescu et al. synthesised monodisperse colloidal $CsPbX_3$ nanocrystals (4–15 nm edge lengths) with cubic shape and cubic perovskite crystal structure by means of the controlled arrested precipitation of Cs^+, Pb^{2+} and X^- ions into $CsPbX_3$.[155] Nanocrystals were obtained by reacting Cs oleate with a Pb^{II}-halide in a high boiling solvent (octadecene) at 140–200 °C. Later on, the same group was able to synthesise a plethora of compounds with band-gap energies and photoluminescence spectra readily tuneable over the entire visible spectral region of 410–700 nm by adjusting the halide ratios in the colloidal nanocrystal solution.[160] Moreover, they compared this synthesis with the analogue for chalcogenide counterparts and fast anion-exchange was observed in perovskite $CsPbX_3$ nanocrystals. XRD patterns showed the retention of the pure cubic phase of the perovskite structure with an average (Scherrer) crystallite size of 8–10 nm. The shift of the XRD reflections was linearly dependent upon the composition (Vegard's law), indicating the formation of uniform solid solutions. The XRD patterns are shown in Figure 9 together with a scheme of the anion-exchange and transmission electron microscopy (TEM) images of about 10 nm $CsPbX_3$ nanocrystals after treatment with various quantities of chloride and iodide anions.

Xiao et al. introduced high pressure step in the synthesis of nanocrystals to tailor the optical and structural properties of $CsPbBr_3$, which is the most thermodynamic stable of the triad. They used a combination of in situ time-resolved carrier dynamics, angle dispersive synchrotron XRD, and optical spectroscopy measurements to determine the optical properties of this pressure-driven structure.[161]

It is known that the presence of chloride during the synthesis of $MAPbI_3$ enhances its air stability and $CsPbCl_3$ presents a robust phase stability.[162] Inspired by that, Dastinar et al. improved the stability of $CsPbI_3$ nanocrystals by incorporating chloride as a dopant.[163] Colloidal nanocrystals of $CsPbI_{3-x}Cl_x$ were synthesised and used in the form of thin films via Kovalenko's group synthesis route.[155] The experimental results were compared with DFT calculations. The doped films showed an enhanced stability toward phase change in humid conditions if compared to the undoped state. Swarnkar et al. further demonstrated the possibility to control the electronic coupling of $CsPbI_3$ colloidal nanocrystals to produce air-stable, efficient solar cells.[164] Figure 10 A, B, D shows the Scheme (with TEM image of quantum dots) and the SEM cross-section of the $CsPbI_3$ cell. Current density/voltage curves show 10.77% PCE for a 0.10 cm^2 cell fully assembled and tested under normal ambient conditions (Figure 10 C).

Although the PCE of the $CsPbBr_3$-based solar cell is limited by a relatively large band-gap, it has been targeted as a potential material for stable high-voltage solar cells.[165] As previously described,[152] the dopant Bi^{3+} is used to extend the range of

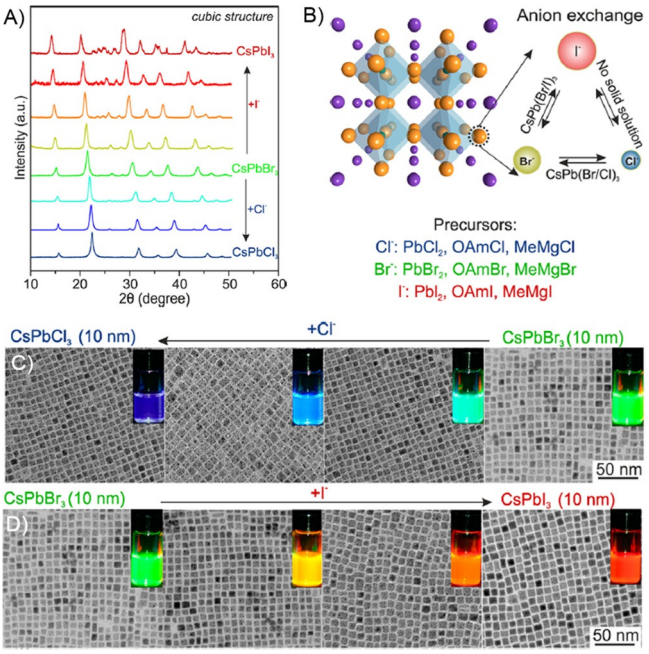

Figure 9. A) Powder XRD patterns of the parent $CsPbBr_3$ nanocrystals and anion-exchanged samples (using $PbCl_2$ and PbI_2 as halide sources), showing the retention of phase pure cubic perovskite structure and an average (Scherrer) crystallite size of 8–10 nm. The shift of the XRD reflections is linearly dependent on the composition (Vegard's law), indicating the formation of uniform solid solutions. B) Schematic of the anion-exchange within the cubic perovskite crystal structure of $CsPbX_3$ along with a list of suitable reagents for each reaction when performed in organic media. C–D) TEM images of ≈10 nm $CsPbX_3$ nanocrystals after treatment with various quantities of chloride (C) and iodide (D) anions. The insets show the evolution of emission colours (under a UV lamp, $\lambda = 365$ nm) upon forming mixed-halide $CsPb(Br/Cl)_3$ and $CsPb(Br/I)_3$ to fully exchanged $CsPbCl_3$ and $CsPbI_3$ nanocrystals. Adapted and reprinted with permission.[160]

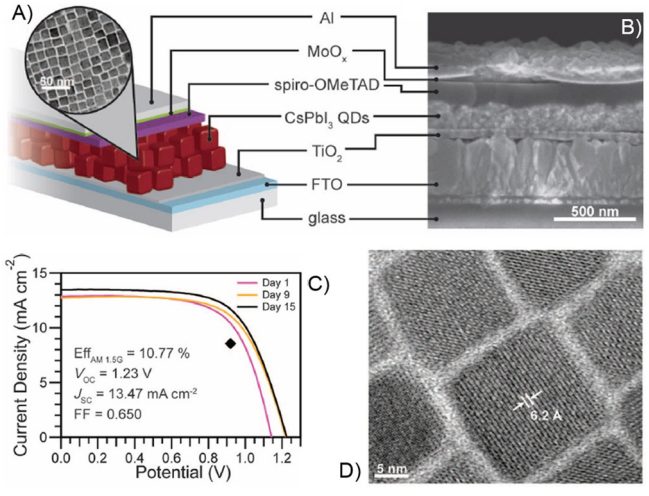

Figure 10. A) Schematic (with TEM image of quantum dots) and B) SEM cross-section of a $CsPbI_3$-based PSC; C) *J-V* curves of a device measured under normal air for 15 days, the black diamond represents the stabilized power output of the device at 0.92 V; D) High-resolution TEM of $CsPbI_3$ quantum dots synthesized at 180 °C. Adapted and reprinted with permission.[164]

the light absorption of $CsPbBr_3$. Although Bi^{3+} has a higher valence than Pb^{2+}, the more similar ionic radius of Bi^{3+} (1.03 Å) and Pb^{2+} (1.19 Å) accounts for the possibility of substitutional doping within the crystal. Miao et al. prepared air stable $CsPbBr_3$ and Bi^{3+}-doped $CsPb_{1-x}Bi_xBr_3$ ($x \ll 1$) single crystals with a cuboid shape via a modified anti-solvent vapour-assisted crystallization method.[166] The scheme of the reaction is summarized in Figure 11 A. The darkness of the synthesised crystals increased proportionally with the amount of inserted Bi^{3+}. As for $CsPbBr_3$, $CsPb_{1-x}Bi_xBr_3$ showed a monocline crystal phase that merely slightly deviated from the cubic perovskite structure of the $Pm\bar{3}m$ (221) space group (Figure 11 B–D). All single crystals exhibited excellent electrical properties, such as low trap density and high carrier mobility, readily comparable to those of the MA-based and FA-based perovskite single crystals.

Caesium precursors for the synthesis of $CsPbBr_3$ have limited solubility in organic solvents, thus making typical solution deposition methods difficult to be adapted to device fabrication.[167] There are few reports on $CsPbBr_3$-based PSCs.[168,169] Hoffman et al. developed a layer-by-layer deposition procedure for bulk $CsPbBr_3$ from fully suspended $CsPbBr_3$ quantum dots that provided controllable thickness and a cubic perovskite crystal structure.[170] This deposition method allowed achieving films with controllable thickness and growth rate in a very simple way. A series of parameters were considered to increase the efficiency of $CsPbBr_3$ PSCs, including the spin-casting solution rate, the annealing temperature and the thickness of the final film. Spin-casting solution at lower concentration required a higher number of deposition cycles. Layered $CsPbBr_3$ solar cells with 6 to 24 deposition cycles provided an improved PCE from 1.35 to 2.25% and from 1.15 to 2.13% for the forward and reverse scan directions, respectively. Modification in the thickness of the active layer was also reported by Akkerman et al.[171] They developed $CsPbBr_3$ perovskite nanocrystal-based solar cells and recorded PCE values ranging from 0.67 to 5.4%.

Panigrahi et al. claimed that the efficient charge transfer process also depends on the generation and extraction of the charge carriers at the interfaces.[172] The perfect band alignment across the layers of the perovskite absorber, ETL and HTL, facilitated the separation of the photoinduced charge carriers and their transportation to the respective electrodes (Figure 12 A). Kelvin probe force microscopy (KPFM) was used to investigate the various charge transfer dynamics at the interfaces of the solar cells under different radiation wavelengths of the full electromagnetic spectrum (white light). They observed the local contact potential difference distribution across the cross-section of the solar cells using a planar ITO/TiO_2/$CsPbBr_3$ quantum dots/spiro-MeOTAD/Au structure (see SEM images in Figure 12 B). Moreover, they investigated the influence of the different radiation spectra on the generation and transport processes of the charge carriers inside the solar cell. The solar cell showed high $V_{oc} = 0.859$ V, $J_{sc} = 8.55$ mA cm^{-2} and FF = 0.57 (Figure 12 C), which led to a PCE of 4.21%.

Recently, a new approach was used to absorb a higher amount of solar radiation than in conventional thin-film

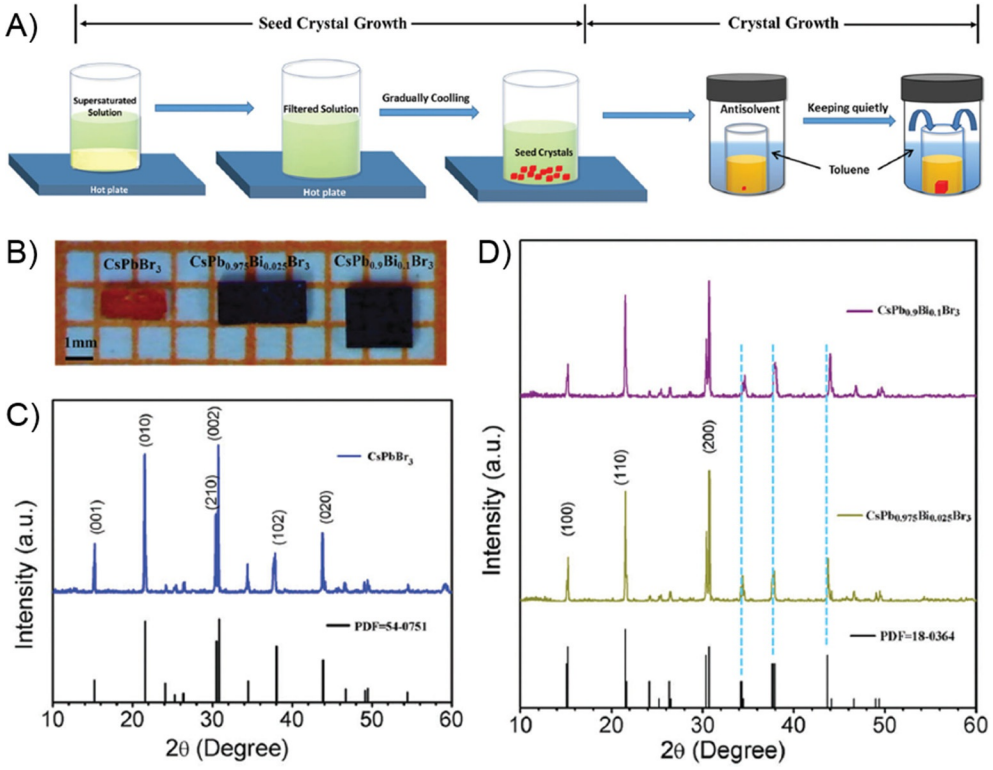

Figure 11. A) Schematic diagram of the crystal growth process; B) Single crystals of $CsPbBr_3$ and $CsPb_xBi_{1-x}Br_3$ prepared by a modified antisolvent vapour-assisted crystallization method; C) XRD patterns of the $CsPbBr_3$ single-crystalline powder; D) XRD patterns of the $CsPb_xBi_{1-x}Br_3$ single-crystalline powders. Adapted and reprinted with permission.[166]

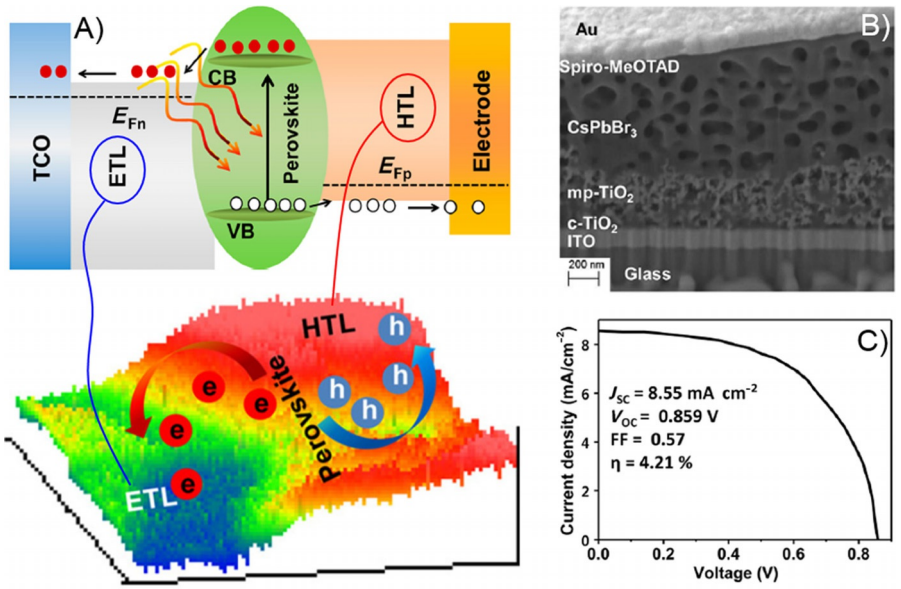

Figure 12. A) Schematic diagram of charge separation in the solar cell under the illumination of the full solar spectrum (white light), together with the scheme of opposite polarities of accumulated charges (electrons and holes) in the two regions (ETL and HTL); B) cross-sectional SEM image and C) *J-V* characteristics and photovoltaic parameters of the solar cell. Adapted and reprinted with permission.[172]

cells.[173] 3D photonic crystals made of close-packed spheres with an inverse opal morphology have attracted increasing attention due to their novel optical features of tuneable photonic stop bands.[174] Zhou et al. combined carbon quantum dots with an inverse opal $CsPbBr_3$ perovskite.[175] They synthesised, for the first time, a carbon quantum dot-embedded $CsPbBr_3$ inverse opal structure through a template-assisted spin-coating method and fabricated efficient PSCs based on the structure of FTO/TiO_2/carbon quantum dots-embedded $CsPbBr_3$ inverse opal/spiro-OMeTAD/Ag. The $CsPbBr_3$ inverse opal exhibited tuneable optical response performance. Iridescent colours to naked eyes arising from the photonic band-gap change of inverse opal structures were clearly notable and, with respect to planar $CsPbBr_3$, this novel active material exhibited a higher PCE equal to 8.29%.

As discussed previously, the problem of solution processing for the $CsPbBr_3$, due to solubility limitations of the bromide ion, was overcome by using the two-step method of Protesescu et al.[155] On this note, Sutton et al. showed that the same method could be condensed in one-step solution processing route and used to partially incorporate Br on $CsPbI_3$.[176] Therefore, the structural stability of $CsPbI_3$ was improved by proper selection of the mixed halide composition of the absorber material. Among the full series of caesium lead halide perovskite ($CsPbI_xBr_{(3-x)}$), $CsPbI_2Br$ demonstrated a perfect combination of ambient stability and suitable band gap (1.92 eV) that makes it a promising material for tandem devices, such as c-Si and CIGS solar cells.[177] Two different device architectures were reported based on c-TiO_2 (compact) and m-TiO_2 (mesoporous). Planar devices showed the highest efficiency, with an average PCE of 6% and two record efficiency devices exceeding 9%. Kennedy et al. carried out further characterization of the $CsPbI_2Br$ perovskite through ultrafast recombination dynamics and excited-state diffusion.[178]

After these encouraging results, $CsPbI_2Br$ attracted remarkable attention in the all-inorganic perovskite research community. Ma et al. investigated the stoichiometric effect on the stability of $CsPbI_2Br$ thin films and devices fabricated by dual source thermal evaporation.[179] They compared the CsBr- and PbI_2-rich $CsPbI_2Br$ devices with the less stable stoichiometrically balanced $CsPbI_2Br$ device. Once encapsulated, $CsPbI_2Br$ provided the best cell PCE performance of 7.7% under reverse scan and a stabilized PCE of 6.7% for a 0.159 cm^2 device. Chen et al. stoichiometrically controlled the $CsPbI_2Br$ perovskite thin films by co-sublimation under high vacuum,[180] achieving a band-gap of 1.82 eV, PCE of 11.8%, high V_{oc} (1.13 V), small hysteresis, and superior thin-film and device stabilities.

According to these results, Nam et al. shed light on the different annealing procedures that cause large variation in the surface morphology and photovoltaic properties.[181] They prepared solution-processed $CsPbI_2Br$ perovskite films by the one-step spin-coating deposition with annealing processes in the range of temperature 100–350 °C. The observation supported the hypothesis that the under- (260 °C) and over-annealed (330 °C) films were chemically unstable against moisture. A comparison proposed by Nam et al. on the different annealing procedures reported in the literature is shown in Table 2[181]. Although their samples were prepared under ambient atmosphere (≈20 °C, RH < 10%), Sutton et al.[177] and Niezgoda et al.[182] performed experiments in an inert gas-filled glovebox to avoid air oxygen and moisture, which may significantly impact on the crystal growth and degradation. Highly efficient planar heterojunction PSCs were obtained by optimal annealing. The device configuration Au/spiro-OMeTAD/$CsPbI_2Br$/blocking-TiO_2/FTO/glass exhibited V_{oc} of 1.23 V and an overall PCE of 10.7%.

Lau et al. demonstrated a low-temperature process to synthesise the $CsPb_{1-x}Sr_xI_2Br$ compound.[184] The incorporation of

Table 2. Comparison of the literature reports on $CsPbI_2Br$ PSCs, with relative most significant photovoltaic parameters. Adapted and reprinted with permission.[181]

Deposition method	Annealing temperature [°C]	V_{oc} [V]	J_{sc} [mA cm^{-2}]	FF	PCE [%]	Ref.
Spin-coating	280 (2 min)	1.20	11.0	0.71	9.4 (10.7)	[181]
Spin-coating	350 (10 min)	0.85	11.8	0.57	6.0 (9.8)	[177]
Spin-coating	1) 65 (5 min) 2) 135 (15 min)	1.12	10.9	–	6.8	[139]
Vacuum co-sublimation	260 (1 min)	1.15	15.2	0.67	11.7 (11.8)	[180]
Spin-coating	280 (10 min)	1.18	10.0	0.70	8.2 (9.5)	[183]
Spin-coating	345 (10 min)	1.08	13.0	0.66	9.2 (10.3)	[182]

strontium (Sr^{2+}) into $CsPbI_2Br$ modified both the electronic and the optical properties of the absorber material, as well as the crystallinity and morphology of the resulting perovskite. Figure 13 A shows the XRD patterns of the $CsPb_{1-x}Sr_xI_2Br$ films, where the characteristic "snowflakes" morphology is clear in the brighter region of SEM images (Figure 13 B–F). The Sr-doped mesoporous PSCs exhibited enhanced performance at Sr = 0.02 molar concentration, resulting in a stabilized PCE of 10.8 % (Figure 13 G, H).

Bai et al. obtained a record efficiency for $CsPbI_2Br$ solar cells (13.47 %, stabilized), by using Mn^{2+} ion doping to modulate film growth and achieving grains with aspect ratios as high as 8.[185] Moreover, Mn^{2+} ions passivated grain boundary and surface defects, leading to a decrease of recombination phenomena and improvement of V_{oc} values up to 1.172 V.

Liang et al. synthesised a novel Cs-based inorganic perovskite, $CsPb_{0.9}Sn_{0.1}IBr_2$, through a convenient two-step sequential solution-phase process in ambient conditions with no need of glovebox or humidity control.[186] The novel material showed suitable band-gap (1.79 eV), close to that of $CsPbI_3$, and superior air stability. Furthermore, they used a new device configuration by replacing the expensive noble metal electrodes with highly stable and conductive carbon electrodes. The FTO/c-TiO_2/*m*-TiO_2/$CsPb_{0.9}Sn_{0.1}IBr_2$/carbon device exhibited an outstandingly high V_{oc} of 1.26 V and a PCE of 11.33 %, as well as a good stability against heat (as high as 100 °C) and humidity.

Replacement of Pb with another group 14 metal, such as Sn or Ge, in all-inorganic PSCs is the new frontier of research to allow PSCs intruding the market on a large-scale in the coming years. Peedikakkandy et al. studied in details the structural and optical properties of Pb-free Sn-based halide perovskites at different compositions.[187] They focused on the calculation, using Kubelka–Munk conversion, of the optical band-gap of these materials. The absorption edge was found to be blue-shifted (from 1.3 to 2.8 eV) upon reducing the size of the anions, that is, from I^- to Br^- to Cl^-, which renders these Pb-free perovskites extremely promising for application in optoelectronic and solar cell devices. Indeed, Sn-based $CsSnI_3$ perovskite was employed in 2012 as the inorganic hole-transporter in solid-state dye-sensitized solar cells (DSSCs).[81] The substitution of Pb with Sn in the lattice reduces toxicity, but worsens the air stability of the resulting materials.[188] On the other hand, using Sn in its stable +4-oxidation state, a deficient Cs_2SnI_6 with a double perovskite structure is obtained. Cs_2SnI_6 has a direct band-gap of 1.3 eV and is more stable versus oxidation and hydrolysis during device processing and operation.[1,189,190] Dolzhnikov et al. used hot injection of Cs oleate (CsOA) into SnI_4 to synthesize quantum/confined Cs_2SnI_6 nanocrystals with band-gaps from 1.38 to 1.47 eV through this reaction [Eq. (1)]:

$$4CsOA + 2SnI_4 \rightarrow Cs_2SnI_6 + 2CsI + Sn(OA)_4 \quad (1)$$

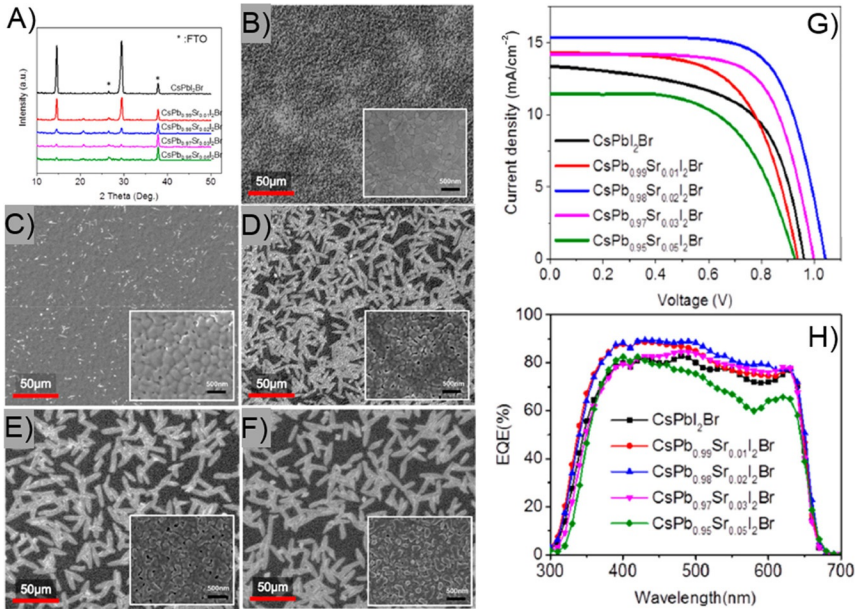

Figure 13. A) XRD patterns of low-temperature-processed $CsPb_{1-x}Sr_xI_2Br$ films. SEM images of B) $CsPbI_2Br$, C) $CsPb_{0.99}Sr_{0.01}I_2Br$, D) $CsPb_{0.98}Sr_{0.02}I_2Br$, E) $CsPb_{0.97}Sr_{0.03}I_2Br$, F) $CsPb_{0.95}Sr_{0.05}I_2Br$; the inset SEM images are taken in the darker region. G) Light *J-V* characteristics under reverse scan and H) external quantum efficiency (EQE) spectra of FTO/c-TiO_2/mp-TiO_2/$CsPb_{1-x}Sr_xI_2Br$/P3HT/Au devices as a function of Sr^{2+} concentration in the perovskite. Adapted and reprinted with permission.[184]

No surfactants were needed to dissolve the Sn precursor, and the diameter of the nanocrystals increased at increasing mixture temperatures. The stability of the colloidal solution upon time was sufficient to allow the deposition of uniform films by simple drop-casting and, consequently, their use in transistors, solar cells and light-emitting diodes (LEDs).[191]

Lee et al. reported a detailed study on the formation of air-stable molecular semiconducting $Cs_2SnI_xBr_{6-x}$ mixed-halide double perovskite.[192] The solid-solution nature of the systems is evidenced by the change of the lattice parameter and the shift of the optical band-gap (Figure 14A). These materials were tested in solid-state Cs_2SnI_6-based cells; the most efficient cell achieved a 2.05% PCE (Figure 14B) and both Cs_2SnI_6 and $Cs_2SnBr_2I_4$ maintained good performances upon air stability tests for 50 days (Figure 14C).

Recently, double perovskites based on bismuth and monovalent metals ($Cs_2BBi^{3+}X_6$, in which B = Cu, Ag, Au) were explored as alternative to lead halide perovskites.[193] Li et al. substituted Pb^{2+} with the trivalent Bi^{3+} cation having the same electronic configuration, and Ag^{+} as second cation.[194] The resulting $Cs_2AgBiBr_6$ double perovskite exhibited an excellent stability and long carrier recombination lifetime. Modulating the pressure during synthesis, they successfully narrowed the band-gap of $Cs_2AgBiBr_6$ from 2.2 to 1.7 eV, accounting for the promising prospects of this newly designed material in Pb-free inorganic PSCs.

Caesium-Doping in Other Perovskite Solar Cell Components

In the previous sections, the fundamental importance of Cs as perovskite doping agent was thoroughly detailed. However, it also plays important roles in a series of other cell components. In particular, Cs modifies the electric transport properties of both ETLs and HTMs.

Mahmud et al. used Cs to improve the properties of solution processed ZnO thin films as ETLs.[195] Indeed, even if they are cheap and facile to prepare at low temperature,[8,196] ZnO ETLs typically exhibit deep trap states due to oxygen chemisorption,[197] which drives the electrons from perovskite LUMO to hop between these trap states before being collected by the back-electrode. As a solution, Mahmud et al. carried out the surface modification of ZnO ETL with Cs-based compounds (acetate and carbonate) to fabricate highly efficient (16.5%) mixed organic cations based $MA_{0.6}FA_{0.4}PbI_3$ PSCs by restricted volume solvent annealing method.[198] Caesium acetate-based ETL demonstrated a 50 meV upshift in the Fermi level position with respect to the carbonate-based counterpart, contributing to higher n-type conductivity and lower electron injection barrier at the interface. In addition, Cs modification profoundly influenced the perovskite microstructure, leading to larger grain size and uniform distribution. The resulting devices demonstrated 400% higher long-term stability if compared to the carbonate-based counterparts, retaining almost 90% of the initial PCE even after 30 days of systematic degradation study.

Among the different PSC device architectures, inverted planar structure is attracting increasing attention due to its low hysteresis, easy setup, and possibility of low temperature processing.[199–201] One of the key issues in this scenario is the performance improvement of HTM in terms of conductivity. Indeed, low conductivity values result in increased recombination phenomena and reduced hole extraction;[202] this drawback can be avoided by either adjusting the stoichiometry of

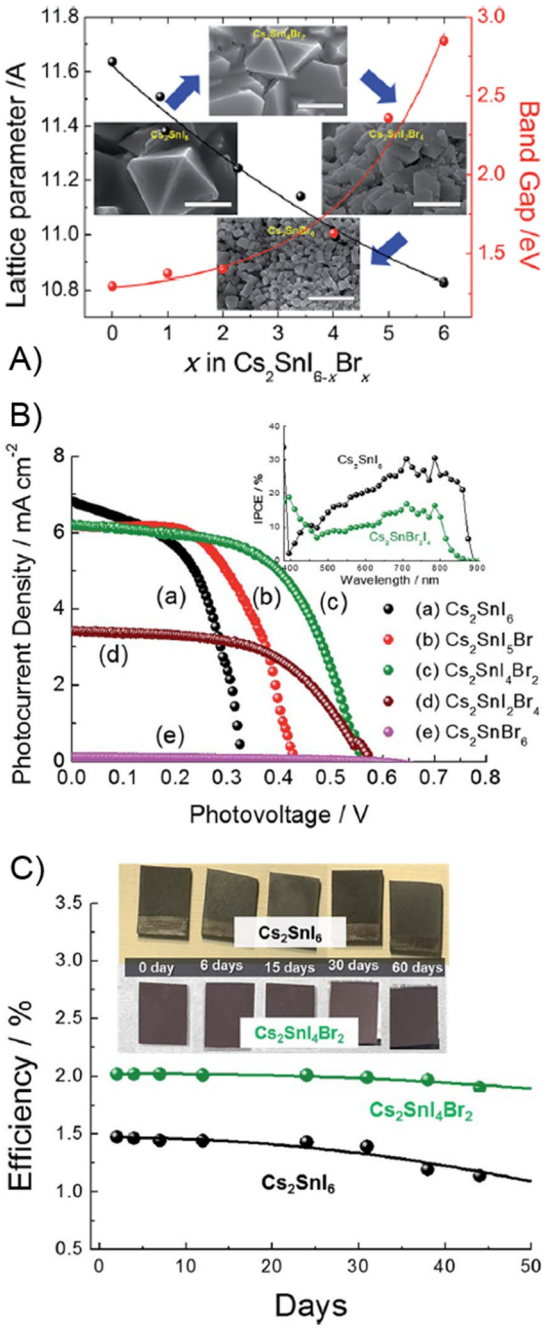

Figure 14. A) Change in the lattice constant and shift in the optical band-gap both indicate the solid-solution nature of the $Cs_2SnI_{6-x}Br_x$ system (inset: surface morphologies of different compounds, with scale bar = 1 mm); B) *J-V* characteristic curves of a series of cells in the "sandwich" configuration with different composition of $Cs_2SnI_{6-x}Br_x$ (inset: IPCE values for Cs_2SnI_6—black—and $Cs_2SnBr_2I_4$—green); C) Stability curves of Cs_2SnI_6 (black) and $Cs_2SnBr_2I_4$ (green) based solar cells upon 50 days aging under air. Adapted and reprinted with permission.[192]

the films or doping, as demonstrated by Chen et al. who studied the impact of Cs dopant on the optoelectronic properties of NiO_x.[203] Smooth, highly transparent films were prepared by the simple solution-based method in the presence of Cs, leading to enhanced electron conductivity and work function. As a result, the solar cell efficiency increased from about 16 to 19%; the best cell provided PCE = 19.35%, also bearing excellent long-term stability (Figure 15A). These remarkable results were attributed to a significant improvement in the hole extraction and a better band alignment compared to undoped NiO_x.

Another possible role for Cs in PSCs is the stabilization of solar cell interfaces. For example, mesoporous and planar heterojunction PSCs typically use a TiO_2 compact layer as the electron collection layer.[6,204] However, upon UV light exposure, photo-generated holes in TiO_2 are very reactive and can induce deep traps leading to charge recombination.[205] To avoid this issue, Li et al. demonstrated that CsCl crystal seeds can markedly enhance the coating of the $CH_3NH_3PbI_{3-x}Cl_x$ absorber layer on TiO_2 in planar heterojunction solar cells.[206] The CsCl modification layer was obtained directly onto the TiO_2 compact layer by spin-coating in water/isopropanol, and led to PCE values up to 16.8%. The CsCl-treated devices maintained 70% of the original PCE after a prolonged (200 min) intensive UV irradiation, definitely outclassing the untreated devices. It was proposed that CsCl likely worked as an UV barrier, whereas other trace amounts of Cs^+ replaced $CH_3NH_3^+$ in the films, thus depressing the generation of CH_3NH_2 and modifying the crystal energy of $CH_3NH_3PbI_{3-x}Cl_x$ (Figure 15B).

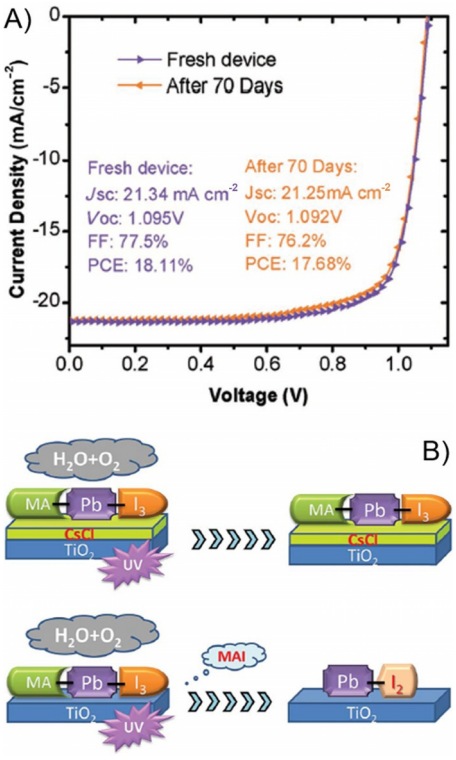

Figure 15. A) *J-V* curves of Cs:NiO_x perovskite devices freshly prepared and after 70 days of storage under inert environments (devices were encapsulated with cover glass, with edge areas sealed with epoxy glue/resin; cells were stored in the glove box and taken outside the glove box only for testing); B) schematic view of the CsCl modification of perovskite thin films in different atmospheres. Adapted and reprinted with permission.[203,206]

The approach described in the previous paragraph is typical (and necessary) for PSCs fabricated with mixed perovskite films because a significant electron transport barrier at the TiO_2/perovskite interface limits their performance. As an alternative, Ye et al. utilized Cs_2CO_3 and CsI as functional enhancers, substantially balancing the electrons and holes transport and increasing the mobility of the carriers.[207] The modified PSCs exhibited reproducible PCE values with little hysteresis in the *J-V* curves, achieving efficiencies up to 19.5 and 20.6% for the Cs_2CO_3-modified and CsI-doped cells, respectively. The dream for PSCs remains that of approaching a stable and reproducible technology because it has also been important for DSSCs[208–221] and other energy-related devices.[222–231]

Caesium-Doped Perovskites in Emerging Technologies

Enhanced optical absorption, long carrier diffusion length and high carrier mobility of perovskite materials can also be exploited in other applications than standard solar cells. Moreover, the integration of PSCs with energy storage systems[232–240] represent a strong research platform for future years.

Waleed et al. demonstrated the application of $CsPbI_3$ nanowires as visible-light photodetectors.[241] The obtained devices, the scheme of which is shown in Figure 16A, delivered quick photoresponse, given by rise and decay times of photocurrent equal to 0.292 and 0.234 s, respectively. Responsivity and specific detectivity reached up to 6.7 mA W^{-1} and 1.57×10^8 Jones under a light intensity of 1.5 mW cm^{-2}. These important figures of merit were attributed mainly to the stabilization of the cubic phase of $CsPbI_3$. It was achieved by the interesting experimental preparation procedure of the nanowires (i.e., chemical vapour deposition method carried out inside anodic alumina membrane), which led to the excellent passivation against intrusion of water molecules as well as nanostructure associated high surface energy.

Cs-based photodetectors were studied also by Ramasamy et al., who described simple, fast and reproducible halide ion exchange reactions in $CsPbX_3$ (X = Cl, Br, I) nanocrystals at room temperature using lithium salts.[242] This preparation technique is rather powerful and allows the fine-tuning of the optical properties of the nanocrystals conceived for optoelectronics applications. The green emission (508 nm) from $CsPbBr_3$ nanocrystals was tuned over the entire visible spectral region (425–655 nm, see Figure 16B) using LiI or LiCl, and the exchange reactions were found to be very fast and proceeded to completion in the order of few seconds. The fabricated photodetectors (Figure 16C,D) exhibited a good on/off photocurrent ratio of 10^5; when the laser was turned on, the photocurrent sharply increased with the applied bias voltage due to the increase in carrier drift velocity. Relatively fast rise (24 ms) and decay times (29 ms) of photocurrent were measured.

Photoluminescence blinking represents another interesting phenomenon where the photophysical properties of Cs-based

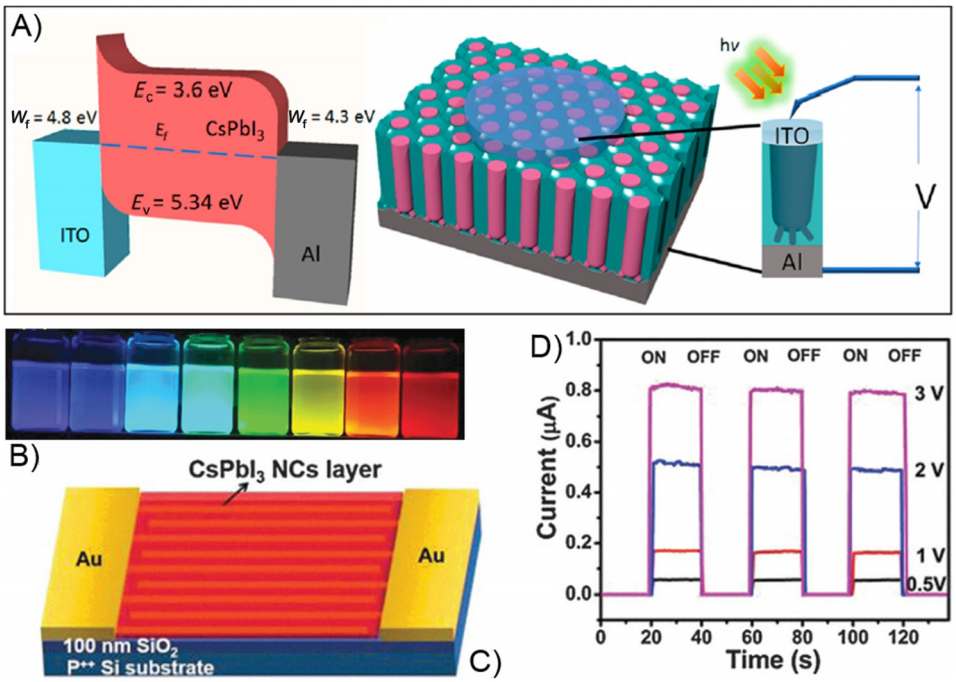

Figure 16. A) Band diagram for $CsPbI_3$ perovskite nanowire-based photodetector device with aluminium and indium-doped tin oxide (ITO) as electrodes (left), schematics of $CsPbI_3$ perovskite nanowire-based device with top circular electrode of ITO having an area of 0.0314 cm^2 (right); B) digital photograph of anion-exchange-synthesized colloidal nanocrystals in hexane under UV lamp ($\lambda = 365$ nm); C) schematics of the resulting $CsPbI_3$-based photodetector and D) photocurrent-time response measured in the dark and under illumination using a laser diode at 405 nm as a function of applied bias at a fixed light intensity (1.98 mW cm^{-2}). Adapted and reprinted with permission.[241,242]

perovskites can be exploited. In this system, the photoluminescence intensity of single emitters randomly switches between bright emissive state and dark non-emissive state under continuous excitation. Zhang et al. proposed colloidal $CsPbX_3$ to this purpose. They regulated the blinking behaviour through varying the halide composition.[243] By means of two different anion-exchange routes (Br^- ions$\rightarrow I^-$ ions and the reverse I^- ions$\rightarrow Br^-$ ions) the interior traps of the perovskite nanocrystals were eliminated, and the resulting alloyed structure reduced the rate of Auger recombination. Under optimized conditions, the authors fabricated "non-blinking" mixed-halide $CsPbBr_{3-y}I_y$ nanocrystals (noteworthy, the "on time" fraction exceeded 99% of the observation time) in a percentage of about 71%.

LEDs, luminescent solar concentrators and related photonic technologies represent other platforms where Cs-based perovskites can behave as core materials in combination with other recently emerged advanced concepts.[244–253] In this scenario, Mn^{2+} doping is currently considered one of the leading strategies to modify the optical and magnetic functionalities of nanocrystals of various chalcogenide and oxide semiconductors.[254] An interesting synergy between these materials chemistry features was proposed by Yuan et al., who synthesized a series of Mn^{2+}-doped $CsPbCl_3$ nanocrystals using reaction temperature and precursor concentration to tune Mn^{2+} content up to 14%.[255] The obtained nanocrystals showed Mn^{2+} $^4T_{1g}\rightarrow{}^6A_{1g}$ d-d luminescence within the optical gap coexisting with excitonic luminescence at the nanocrystals absorption edge, and quantum yields up to 62% were observed for Mn^{2+} concentrations of about 3%. The obtained photophysical properties of these Cs-based perovskites resulted in a new class of doped semiconductor nanocrystals bearing potential nanophosphor applications.

In the framework of light-induced effects in advances materials,[256–264] photoluminescence probes for metal ions represent another challenging application for Cs-based perovskites. Indeed, due to the significance of metal ions in biological and industrial systems, demand is growing for strategies of trace metal ions probing under various conditions. For this purpose, Sheng et al. proposed $CsPbX_3$ quantum dots as Cu^{2+} and Yb^{3+} probe with high sensitivity, high selectivity and instant response through the quenching or enhancement of the photoluminescence.[265] Impressively, the probing limit for Cu^{2+} and Yb^{3+} ions were as low as sub-2×10^{-9} and ranged up to 2×10^{-5} M. This finding nowadays represents a competitive strategy to detect metal ions in biological and industrial organic systems, especially for those species (like rare earth ions) that are nutritionally essential and medically important for a healthy life, but only at low levels.

It is reasonable thinking that the current efforts in developing novel perovskite nanostructures will be soon a precious resource in the field of sensors, electronics and energy-related devices.[266–275]

Conclusions

In this article, we reviewed the most significant improvements in stability, reproducibility and spectral properties of perovskite solar cells achieved by the scientific community through Cs-

doping. In this respect, the scientific community is currently focused on developing both hybrid organic–inorganic and inorganic perovskite solar cells being stable upon long-term operation, and this might be achieved by appropriate synthetic strategies, optimized compositions and in-depth analysis of crystallographic parameters.[276–281]

At this point of development, thanks to Cs-doping, the perovskites-based photovoltaic technology can rely on reproducible and consolidated preparation procedures of the active materials, which represent a fundamental milestone in view of their widespread diffusion. Future studies should be devoted to identifying novel preparation techniques likely under ambient conditions and optimization thereof towards production and commercialization of modules on a large-scale.

Acknowledgements

F.B. thanks Politecnico di Torino and Compagnia di San Paolo for the financial support through the call "Metti in rete la tua idea di ricerca" (PEPPY project).

Conflict of interest

The authors declare no conflict of interest.

Keywords: caesium · doping · hybrid perovskite · perovskite solar cell · photovoltaics

[1] J. Burschka, N. Pellet, S. J. Moon, R. Humphry-Baker, P. Gao, M. K. Nazeeruddin, M. Grätzel, *Nature* **2013**, *499*, 316 – 319.
[2] M. Liu, M. B. Johnston, H. J. Snaith, *Nature* **2013**, *501*, 395 – 398.
[3] H. S. Kim, C. R. Lee, J. H. Im, K. B. Lee, T. Moehl, A. Marchioro, S. J. Moon, R. Humphry-Baker, J. H. Yum, J. E. Moser, M. Grätzel, N. G. Park, *Sci. Rep.* **2012**, *2*, 591.
[4] H. Zhou, Q. Chen, G. Li, S. Luo, T. B. Song, H. S. Duan, Z. Hong, J. You, Y. Liu, Y. Yang, *Science* **2014**, *345*, 542 – 546.
[5] N. J. Jeon, J. H. Noh, Y. C. Kim, W. S. Yang, S. Ryu, S. I. Seok, *Nat. Mater.* **2014**, *13*, 897 – 903.
[6] N. J. Jeon, J. H. Noh, W. S. Yang, Y. C. Kim, S. Ryu, J. Seo, S. I. Seok, *Nature* **2015**, *517*, 476 – 480.
[7] J. H. Heo, S. H. Im, J. H. Noh, T. N. Mandal, C. S. Lim, J. A. Chang, Y. H. Lee, H. J. Kim, A. Sarkar, M. K. Nazeeruddin, M. Grätzel, S. I. Seok, *Nat. Photonics* **2013**, *7*, 486 – 491.
[8] D. Liu, T. L. Kelly, *Nat. Photonics* **2014**, *8*, 133 – 138.
[9] Q. Chen, H. Zhou, Z. Hong, S. Luo, H. S. Duan, H. H. Wang, Y. Liu, G. Li, Y. Yang, *J. Am. Chem. Soc.* **2014**, *136*, 622 – 625.
[10] G. E. Eperon, V. M. Burlakov, P. Docampo, A. Goriely, H. J. Snaith, *Adv. Funct. Mater.* **2014**, *24*, 151 – 157.
[11] I. Pecnikaj, D. Minudri, L. Otero, F. Fungo, M. Cavazzini, S. Orlandi, G. Pozzi, *New J. Chem.* **2017**, *41*, 7729 – 7738.
[12] E. Andrzejewska, A. Marcinkowska, A. Zgrzeba, *Polimery* **2017**, *62*, 344 – 352.
[13] S. Yang, H. C. Su, J. L. Hou, W. Luo, D. H. Zou, Q. Y. Zhu, J. Dai, *Dalton Trans.* **2017**, *46*, 9639 – 9645.
[14] S. Chowdhury, R. Balasubramanian, *Prog. Mater. Sci.* **2017**, *90*, 224 – 275.
[15] H. Gupta, K. Shalu, L. Balo, V. K. Singh, S. K. Singh, A. K. Tripathi, Y. L. Verma, R. K. Singh, *Solid State Ionics* **2017**, *309*, 192 – 199.
[16] L. Qiu, L. K. Ono, Y. Qi, *Mater. Today Energy* **2018**, *7*, 169 – 189.
[17] M. Wang, J. Bian, Y. Feng, Y. Zhang, H. Liu, Y. Shi, *Mater. Sci. Semicond. Process.* **2018**, *80*, 131 – 136.
[18] M. Wang, J. Bian, Y. Feng, Q. Dong, B. Zhang, H. Liu, Y. Shi, *Mater. Sci. Semicond. Process.* **2018**, *80*, 174 – 178.
[19] J. Huang, C. Wang, Z. Liu, X. Qiu, J. Yang, J. Chang, *J. Mater. Chem. C* **2018**, *6*, 2311 – 2318.
[20] F. U. Kosasih, C. Ducati, *Nano Energy* **2018**, *47*, 243 – 256.
[21] J. Nakazaki, H. Segawa, *J. Photochem. Photobiol. C* **2018**, *35*, 74 – 107.
[22] Y. Chen, L. Zhang, Y. Zhang, H. Gao, H. Yan, *RSC Adv.* **2018**, *8*, 10489 – 10508.
[23] P. Zhao, M. Han, W. Yin, X. Zhao, S. G. Kim, Y. Yan, M. Kim, Y. J. Song, N. G. Park, H. S. Jung, *ACS Appl. Mater. Interfaces* **2018**, *10*, 10132 – 10140.
[24] Z. Li, T. R. Klein, D. H. Kim, M. Yang, J. J. Berry, M. F. A. M. Van Hest, K. Zhu, *Nat. Rev. Mater.* **2018**, *3*, 18017.
[25] H. S. Roh, G. S. Han, S. Lee, S. Kim, S. Choi, C. Yoon, J. K. Lee, *J. Power Sources* **2018**, *389*, 135 – 139.
[26] J. Xie, V. Arivazhagan, K. Xiao, K. Yan, Z. Yang, Y. Qiang, P. Hang, G. Li, C. Cui, X. Yu, D. Yang, *J. Mater. Chem. A* **2018**, *6*, 5566 – 5573.
[27] A. Tiihonen, K. Miettunen, J. Halme, S. Lepikko, A. Poskela, P. D. Lund, *Energy Environ. Sci.* **2018**, *11*, 730 – 738.
[28] J. Chen, D. Lee, N. G. Park, *ACS Appl. Mater. Interfaces* **2017**, *9*, 36338 – 36349.
[29] H. Li, Y. Li, Y. Li, J. Shi, H. Zhang, X. Xu, J. Wu, H. Wu, Y. Luo, D. Li, Q. Meng, *Nano Energy* **2017**, *42*, 222 – 231.
[30] Y. Zhang, J. Wang, X. Liu, W. Li, F. Huang, Y. Peng, J. Zhong, Y. Cheng, Z. Ku, *RSC Adv.* **2017**, *7*, 48958 – 48961.
[31] I. Jeong, Y. H. Park, S. Bae, M. Park, H. Jeong, P. Lee, M. J. Ko, *ACS Appl. Mater. Interfaces* **2017**, *9*, 36865 – 36874.
[32] Z. Ahmad, M. A. Najeeb, R. A. Shakoor, A. Alashraf, S. A. Al-Muhtaseb, A. Soliman, M. K. Nazeeruddin, *Sci. Rep.* **2017**, *7*, 15406.
[33] H. Zheng, G. Liu, L. Zhu, J. Ye, X. Zhang, A. Alsaedi, T. Hayat, X. Pan, S. Dai, *ACS Appl. Mater. Interfaces* **2017**, *9*, 41006 – 41013.
[34] N. Rolston, A. D. Printz, F. Hilt, M. Q. Hovish, K. Brüning, C. J. Tassone, R. H. Dauskardt, *J. Mater. Chem. A* **2017**, *5*, 22975 – 22983.
[35] W. M. Guo, M. Zhong, *Chinese J. Inorg. Chem.* **2017**, *33*, 1097 – 1118.
[36] A. Gheno, T. Trigaud, J. Bouclé, P. Audebert, B. Ratier, S. Vedraine, *Opt. Mater.* **2018**, *75*, 781 – 786.
[37] E. Ercan, J. Y. Chen, P. C. Tsai, J. Y. Lam, S. C. W. Huang, C. C. Chueh, W. C. Chen, *Adv. Electron. Mater.* **2017**, *3*, 1700344.
[38] S. Wang, C. Bi, J. Yuan, L. Zhang, J. Tian, *ACS Energy Lett.* **2018**, *3*, 245 – 251.
[39] L. Qiu, L. K. Ono, Y. Jiang, M. R. Leyden, S. R. Raga, S. Wang, Y. Qi, *J. Phys. Chem. B* **2018**, *122*, 511 – 520.
[40] T. P. Nguyen, A. Ozturk, J. Park, W. Sohn, T. H. Lee, H. W. Jang, S. Y. Kim, *Sci. Technol. Adv. Mater.* **2018**, *19*, 10 – 17.
[41] N. N. Shlenskaya, N. A. Belich, M. Grätzel, E. A. Goodilin, A. B. Tarasov, *J. Mater. Chem. A* **2018**, *6*, 1780 – 1786.
[42] Z. Zhu, D. Zhao, C. C. Chueh, X. Shi, Z. Li, A. K. Y. Jen, *Joule* **2018**, *2*, 168 – 183.
[43] L. B. Huang, P. Y. Su, J. M. Liu, J. F. Huang, Y. F. Chen, S. Qin, J. Guo, Y. W. Xu, C. Y. Su, *J. Power Sources* **2018**, *378*, 483 – 490.
[44] W. Zhang, P. Liu, A. Sadollahkhani, Y. Li, B. Zhang, F. Zhang, M. Safdari, Y. Hao, Y. Hua, L. Kloo, *ACS Omega* **2017**, *2*, 9231 – 9240.
[45] M. Anaya, G. Lozano, M. E. Calvo, H. Míguez, *Joule* **2017**, *1*, 769 – 793.
[46] W. Deng, X. Liang, P. S. Kubiak, P. J. Cameron, *Adv. Energy Mater.* **2018**, *8*, 1701544.
[47] Z. Wu, B. Sun, *Sci. China Mater.* **2018**, *61*, 125 – 126.
[48] M. I. H. Ansari, A. Qurashi, M. K. Nazeeruddin, *J. Photochem. Photobiol. C* **2018**, *35*, 1 – 24.
[49] J. Luo, Y. Wang, Q. Zhang, *Sol. Energy* **2018**, *163*, 289 – 306.
[50] A. Dubey, N. Adhikari, S. Mabrouk, F. Wu, K. Chen, S. Yang, Q. Qiao, *J. Mater. Chem. A* **2018**, *6*, 2406 – 2431.
[51] A. Fakharuddin, L. Schmidt-Mende, G. Garcia-Belmonte, R. Jose, I. Mora-Sero, *Adv. Energy Mater.* **2017**, *7*, 1700623.
[52] J. P. Correa-Baena, M. Saliba, T. Buonassisi, M. Grätzel, A. Abate, W. Tress, A. Hagfeldt, *Science* **2017**, *358*, 739 – 744.
[53] H. S. Jung, N. G. Park, *Small* **2015**, *11*, 10 – 25.
[54] N. G. Park, *Mater. Today* **2015**, *18*, 65 – 72.
[55] T. A. Berhe, W. N. Su, C. H. Chen, C. J. Pan, J. H. Cheng, H. M. Chen, M. C. Tsai, L. Y. Chen, A. A. Dubale, B. J. Hwang, *Energy Environ. Sci.* **2016**, *9*, 323 – 356.
[56] Y. Zhao, K. Zhu, *J. Phys. Chem. Lett.* **2014**, *5*, 4175 – 4186.

[57] T. Miyasaka, *Chem. Lett.* **2015**, *44*, 720 – 729.
[58] X. Li, X. Zhong, Y. Hu, B. Li, Y. Sheng, Y. Zhang, C. Weng, M. Feng, H. Han, J. Wang, *J. Phys. Chem. Lett.* **2017**, *8*, 1804 – 1809.
[59] M. Cheraghizade, F. Jamali-Sheini, R. Yousefi, *Appl. Phys. A* **2017**, *123*, 390.
[60] B. Klöckner, K. Niederer, A. Fokina, H. Frey, R. Zentel, *Macromolecules* **2017**, *50*, 3779 – 3788.
[61] J. H. Li, Y. Li, J. T. Xu, C. K. Luscombe, *ACS Appl. Mater. Interfaces* **2017**, *9*, 17942 – 17948.
[62] D. Wood, E. Capuzzo, D. Kirby, K. Mooney-McAuley, P. Kerrison, *Mar. Policy* **2017**, *83*, 29 – 39.
[63] A. Abate, J. P. Correa-Baena, M. Saliba, M. S. Su'ait, F. Bella, *Chem. Eur. J.* **2018**, *24*, 3083 – 3100.
[64] M. Wang, Y. Feng, J. Bian, H. Liu, Y. Shi, *Chem. Phys. Lett.* **2018**, *692*, 44 – 49.
[65] W. Tan, A. R. Bowring, A. C. Meng, M. D. McGehee, P. C. McIntyre, *ACS Appl. Mater. Interfaces* **2018**, *10*, 5485 – 5491.
[66] Z. Zhang, K. Xu, X. Rong, Y. S. Hu, H. Li, X. Huang, L. Chen, *J. Power Sources* **2017**, *372*, 270 – 275.
[67] H. Fei, N. Saha, N. Kazantseva, R. Moucka, Q. Cheng, P. Saha, *Materials* **2017**, *10*, 1251.
[68] X. Su, K. Guo, T. Ma, P. A. Tamirisa, H. Ye, H. Gao, B. W. Sheldon, *ACS Energy Lett.* **2017**, *2*, 1729 – 1733.
[69] X. Wang, H. Zhu, G. M. A. Girard, R. Yunis, D. R. Macfarlane, D. Mecerreyes, A. J. Bhattacharyya, P. C. Howlett, M. Forsyth, *J. Mater. Chem. A* **2017**, *5*, 23844 – 23852.
[70] Q. Ma, Y. Hu, H. Li, L. Chen, X. Huang, Z. Zhou, *Acta Phys. Chim. Sin.* **2018**, *34*, 213 – 218.
[71] C. Jiang, H. Li, C. Wang, *Sci. Bull.* **2017**, *62*, 1473 – 1490.
[72] Y. Ma, J. Ma, J. Chai, Z. Liu, G. Ding, G. Xu, H. Liu, B. Chen, X. Zhou, G. Cui, L. Chen, *ACS Appl. Mater. Interfaces* **2017**, *9*, 41462 – 41472.
[73] R. Muthupradeepa, M. Sivakumar, R. Subadevi, V. Suryanarayanan, W. R. Liu, *J. Nanosci. Nanotechnol.* **2018**, *18*, 215 – 222.
[74] B. Huang, Y. Zhang, M. Que, Y. Xiao, Y. Jiang, K. Yuan, Y. Chen, *RSC Adv.* **2017**, *7*, 54391 – 54398.
[75] Y. C. Jung, M. S. Park, D. H. Kim, M. Ue, A. Eftekhari, D. W. Kim, *Sci. Rep.* **2017**, *7*, 17482.
[76] A. Kojima, K. Teshima, Y. Shirai, T. Miyasaka, *J. Am. Chem. Soc.* **2009**, *131*, 6050 – 6051.
[77] G. Xing, N. Mathews, S. Sun, S. S. Lim, Y. M. Lam, M. Gratzel, S. Mhaisalkar, T. C. Sum, *Science* **2013**, *342*, 344 – 347.
[78] M. Grätzel, *Nat. Mater.* **2014**, *13*, 838 – 842.
[79] M. M. Lee, J. Teuscher, T. Miyasaka, T. N. Murakami, H. J. Snaith, *Science* **2012**, *338*, 643 – 647.
[80] S. D. Stranks, G. E. Eperon, G. Grancini, C. Menelaou, M. J. P. Alcocer, T. Leijtens, L. M. Herz, A. Petrozza, H. J. Snaith, *Science* **2013**, *342*, 341 – 344.
[81] I. Chung, B. Lee, J. He, R. P. H. Chang, M. G. Kanatzidis, *Nature* **2012**, *485*, 486 – 489.
[82] J. H. Im, C. R. Lee, J.-. Lee, S. W. Park, N. G. Park, *Nanoscale* **2011**, *3*, 4088 – 4093.
[83] Z. Cheng, J. Lin, *CrystEngComm* **2010**, *12*, 2646 – 2662.
[84] R. K. Misra, S. Aharon, B. Li, D. Mogilyansky, I. Visoly-Fisher, L. Etgar, E. A. Katz, *J. Phys. Chem. Lett.* **2015**, *6*, 326 – 330.
[85] Y. Zhang, S. Chen, P. Xu, H. Xiang, X. Gong, A. Walsh, S. Wei, *Chin. Phys. Lett.* **2018**, *35*, 036104.
[86] B. J. Foley, D. L. Marlowe, K. Sun, W. A. Saidi, L. Scudiero, M. C. Gupta, J. Choi, *Appl. Phys. Lett.* **2015**, *106*, 243904.
[87] E. T. Hoke, D. J. Slotcavage, E. R. Dohner, A. R. Bowring, H. I. Karunadasa, M. D. McGehee, *Chem. Sci.* **2015**, *6*, 613 – 617.
[88] C. C. Stoumpos, C. D. Malliakas, M. G. Kanatzidis, *Inorg. Chem.* **2013**, *52*, 9019 – 9038.
[89] J. Lee, D. Seol, A. Cho, N. Park, *Adv. Mater.* **2014**, *26*, 4991 – 4998.
[90] Z. Xiao, Y. Yuan, Y. Shao, Q. Wang, Q. Dong, C. Bi, P. Sharma, A. Gruverman, J. Huang, *Nat. Mater.* **2015**, *14*, 193 – 198.
[91] H. Choi, J. Jeong, H. B. Kim, S. Kim, B. Walker, G. H. Kim, J. Y. Kim, *Nano Energy* **2014**, *7*, 80 – 85.
[92] J. A. Koza, J. C. Hill, A. C. Demster, J. A. Switzer, *Chem. Mater.* **2016**, *28*, 399 – 405.
[93] E. Mosconi, E. Ronca, F. De Angelis, *J. Phys. Chem. Lett.* **2014**, *5*, 2619 – 2625.
[94] J. Yin, D. Cortecchia, A. Krishna, S. Chen, N. Mathews, A. C. Grimsdale, C. Soci, *J. Phys. Chem. Lett.* **2015**, *6*, 1396 – 1402.
[95] Q. Liang, J. Liu, Z. Cheng, Y. Li, L. Chen, R. Zhang, J. Zhang, Y. Han, *J. Mater. Chem. A* **2016**, *4*, 223 – 232.
[96] S. Bae, S. J. Han, T. J. Shin, W. H. Jo, *J. Mater. Chem. A* **2015**, *3*, 23964 – 23972.
[97] G. Niu, H. Yu, J. Li, D. Wang, L. Wang, *Nano Energy* **2016**, *27*, 87 – 94.
[98] G. Niu, W. Li, J. Li, X. Liang, L. Wang, *RSC Adv.* **2017**, *7*, 17473 – 17479.
[99] Y. Zhou, Z. Zhou, M. Chen, Y. Zong, J. Huang, S. Pang, N. P. Padture, *J. Mater. Chem. A* **2016**, *4*, 17623 – 17635.
[100] M. Saliba, T. Matsui, K. Domanski, J. Y. Seo, A. Ummadisingu, S. M. Zakeeruddin, J. P. Correa-Baena, W. R. Tress, A. Abate, H. Hagfeldt, M. Grätzel, *Science* **2016**, *354*, 206 – 209.
[101] S. Pang, H. Hu, J. Zhang, S. Lv, Y. Yu, F. Wei, T. Qin, H. Xu, Z. Liu, G. Cui, *Chem. Mater.* **2014**, *26*, 1485 – 1491.
[102] F. Meillaud, A. Shah, C. Droz, E. Vallat-Sauvain, C. Miazza, *Sol. Energy Mater. Sol. Cells* **2006**, *90*, 2952 – 2959.
[103] V. M. Goldschmidt, *Naturwiss.* **1926**, *14*, 477 – 485.
[104] C. C. Stoumpos, M. G. Kanatzidis, *Acc. Chem. Res.* **2015**, *48*, 2791 – 2802.
[105] Z. Li, M. Yang, J. S. Park, S. H. Wei, J. J. Berry, K. Zhu, *Chem. Mater.* **2016**, *28*, 284 – 292.
[106] X. Xia, W. Wu, H. Li, B. Zheng, Y. Xue, J. Xu, D. Zhang, C. Gaob, X. Liu, *RSC Adv.* **2016**, *6*, 14792 – 14798.
[107] T. Liu, Y. Zong, Y. Zhou, M. Yang, Z. Li, O. S. Game, K. Zhu, R. Zhu, Q. Gong, N. P. Padture, *Chem. Mater.* **2017**, *29*, 3246 – 3250.
[108] Y. H. Chiang, M. H. Li, H. M. Cheng, P. S. Shen, P. Chen, *ACS Appl. Mater. Interfaces* **2017**, *9*, 2403 – 2409.
[109] L. Y. Zhang, Y. Zhang, W. B. Guan, K. F. Wang, Z. X. Cheng, Y. X. Wang, *J. Mater. Sci.* **2017**, *52*, 13203 – 13211.
[110] W. Zhu, C. Bao, F. Li, T. Yu, H. Gao, Y. Yi, J. Yang, G. Fu, X. Zhou, Z. Zou, *Nano Energy* **2016**, *19*, 17 – 26.
[111] R. G. Niemann, L. Gouda, J. Hu, S. Tirosh, R. Gottesman, P. J. Cameron, A. Zaban, *J. Mater. Chem. A* **2016**, *4*, 17819 – 17827.
[112] Y. Tu, J. Wu, Z. Lan, X. He, J. Dong, J. Jia, P. Guo, J. Lin, M. Huang, Y. Huang, *Sci. Rep.* **2017**, *7*, 44603.
[113] M. Saliba, T. Matsui, J. Y. Seo, K. Domanski, J. P. Correa-Baena, M. K. Nazeeruddin, S. M. Zakeeruddin, W. Tress, A. Abate, A. Hagfeldt, M. Grätzel, *Energy Environ. Sci.* **2016**, *9*, 1989 – 1997.
[114] M. Deepa, M. Salado, L. Calio, S. Kazim, S. M. Shivaprasad, S. Ahmad, *Phys. Chem. Chem. Phys.* **2017**, *19*, 4069 – 4077.
[115] M. Salado, R. K. Kokal, L. Calio, S. Kazim, M. Deepa, S. Ahmad, *Phys. Chem. Chem. Phys.* **2017**, *19*, 22905 – 22914.
[116] R. Hamaguchi, M. Yoshizawa-Fujita, T. Miyasaka, H. Kunugita, K. Ema, Y. Takeoka, M. Rikukawa, *Chem. Commun.* **2017**, *53*, 4366 – 4369.
[117] D. J. Slotcavage, H. I. Karunadasa, M. D. McGehee, *ACS Energy Lett.* **2016**, *1*, 1199 – 1205.
[118] L. K. Ono, Y. Qi, *J. Phys. Chem. Lett.* **2016**, *7*, 4764 – 4794.
[119] N. Li, Z. Zhu, Q. Dong, J. Li, Z. Yang, C. C. Chueh, A. K. Y. Jen, L. Wang, *Adv. Mater. Interfaces* **2017**, *4*, 1700598.
[120] X. Zhang, X. Ren, B. Liu, R. Munir, X. Zhu, D. Yang, J. Li, Y. Liu, D. M. Smilgies, R. Li, Z. Yang, T. Niu, X. Wang, A. Amassian, K. Zhao, S. F. Liu, *Energy Environ. Sci.* **2017**, *10*, 2095 – 2102.
[121] H. Tsai, W. Nie, J. C. Blancon, C. C. Stoumpos, R. Asadpour, B. Harutyunyan, A. J. Neukirch, R. Verduzco, J. J. Crochet, S. Tretiak, L. Pedesseau, J. Even, M. A. Alam, G. Gupta, J. Lou, P. M. Ajayan, M. J. Bedzyk, M. G. Kanatzidis, A. D. Mohite, *Nature* **2016**, *536*, 312 – 316.
[122] Z. Wang, Q. Lin, F. P. Chmiel, N. Sakai, L. M. Herz, H. J. Snaith, *Nat. Energy* **2017**, *2*, 17135.
[123] Y. Shao, Z. Xiao, C. Bi, Y. Yuan, J. Huang, *Nat. Commun.* **2014**, *5*, 5784.
[124] E. Mosconi, P. Umari, F. D. Angelis, *J. Mater. Chem. A* **2015**, *3*, 9208 – 9215.
[125] F. Hao, C. C. Stoumpos, R. P. H. Chang, M. G. Kanatzidis, *J. Am. Chem. Soc.* **2014**, *136*, 8094 – 8099.
[126] M. Anaya, J. P. Correa-Baena, G. Lozano, M. Saliba, P. Anguita, B. Roose, A. Abate, U. Steiner, M. Grätzel, M. E. Calvo, A. Hagfeldt, H. Mìguz, *J. Mater. Chem. A* **2016**, *4*, 11214 – 11221.
[127] F. Hao, C. C. Stoumpos, D. H. Cao, R. P. H. Chang, M. G. Kanatzidis, *Nat. Photonics* **2014**, *8*, 489 – 494.
[128] Z. Yang, A. Rajagopal, C. C. Chueh, S. B. Jo, B. Liu, T. Zhao, A. K. Y. Jen, *Adv. Mater.* **2016**, *28*, 8990 – 8997.

[129] X. Liu, Z. Yang, C. C. Chueh, A. Rajagopal, S. T. Williams, Y. Sunb, A. K. Y. Jen, *J. Mater. Chem. A* **2016**, *4*, 17939 – 17945.
[130] J. W. Lee, D. H. Kim, H. S. Kim, S. W. Seo, S. M. Cho, N. G. Park, *Adv. Energy Mater.* **2015**, *5*, 1501310.
[131] P. Qin, S. Tanaka, S. Ito, N. Tetreault, K. Manabe, H. Nishino, M. K. Nazeeruddin, M. Grätzel, *Nat. Commun.* **2014**, *5*, 3834.
[132] G. Murugadoss, G. Mizuta, S. Tanaka, H. Nishino, T. Umeyama, H. Imahori, S. Ito, *APL Mater.* **2014**, *2*, 081511.
[133] G. Murugadoss, R. Thangamuthu, S. Vijayaraghavan, H. Kanda, S. Ito, *Electrochim. Acta* **2017**, *257*, 267 – 280.
[134] P. Luo, S. Zhou, Y. Zhou, W. Xia, L. Sun, J. Cheng, C. Xu, Y. Lu, *ACS Appl. Mater. Interfaces* **2017**, *9*, 42708 – 42716.
[135] T. Ye, S. L. Lim, X. Li, M. Petrović, X. Wang, C. Jiang, W. P. Goh, C. Vijila, S. Ramakrishna, *Sol. Energy Mater. Sol. Cells* **2018**, *175*, 111 – 117.
[136] P. P. Boix, K. Nonomura, N. Mathews, S. G. Mhaisalkar, *Mater. Today* **2014**, *17*, 16 – 23.
[137] B. Brunetti, C. Cavallo, A. Ciccioli, G. Gigli, A. Latini, *Sci. Rep.* **2016**, *6*, 31896.
[138] M. Kulbak, D. Cahen, G. Hodes, *J. Phys. Chem. Lett.* **2015**, *6*, 2452 – 2456.
[139] R. E. Beal, D. J. Slotcavage, T. Leijtens, A. R. Bowring, R. A. Belisle, W. H. Nguyen, G. F. Burkhard, E. T. Hoke, M. D. McGehee, *J. Phys. Chem. Lett.* **2016**, *7*, 746 – 751.
[140] Y. Hu, E. M. Hutter, P. Rieder, I. Grill, J. Hanisch, M. F. Aygüler, A.G. Hufnagel, M. Handloser, T. Bein, A. Hartschuh, K. Tvingstedt, V. Dyakonov, A. Baumann, T. J. Savenije, M.L. Petrus, P. Docampo, *Adv. Energy Mater.* **2018**, *8*, 1703057.
[141] Y. Hu, M. F. Aygüler, M. L. Petrus, T. Bein, P. Docampo, *ACS Energy Lett.* **2017**, *2*, 2212 – 2218.
[142] R. X. Yang, J. M. Skelton, E. Lora da Silva, J. M. Frost, A. Walsh, *J. Phys. Chem. Lett.* **2017**, *8*, 4720 – 4726.
[143] H. L. Wells, *Z. Anorg. Chem.* **1893**, *3*, 195 – 210.
[144] C. K. Møller, *Nature* **1958**, *182*, 1436 – 1436.
[145] A. Marronnier, G. Roma, S. Boyer-Richard, L. Pedesseau, J. M. Jancu, Y. Bonnassieux, C. Katan, C. C. Stoumpos, M. G. Kanatzidis, J. Even, *ACS Nano* **2018**, *12*, 3477 – 3486.
[146] J. Liang, C. Wang, Y. Wang, Z. Xu, Z. Lu, Y. Ma, H. Zhu, Y. Hu, C. Xiao, X. Yi, G. Zhu, H. Lv, L. Ma, T. Chen, Z. Tie, Z. Jin, J. Liu, *J. Am. Chem. Soc.* **2016**, *138*, 15829 – 15832.
[147] C. C. Stoumpos, C. D. Malliakas, J. A. Peters, Z. Liu, M. Sebastian, J. Im, T. C. Chasapis, A. C. Wibowo, D. Y. Chung, A. J. Freeman, B. W. Wessels, M. G. Kanatzidis, *Cryst. Growth Des.* **2013**, *13*, 2722 – 2727.
[148] S. Sharma, N. Weiden, A. Weiss, *Z. Phys. Chem.* **1992**, *175*, 63 – 80.
[149] M. Lai, Q. Kong, C. G. Bischak, Y. Yu, L. Dou, S. W. Eaton, N. S. Ginsberg, P. Yang, *Nano Res.* **2017**, *10*, 1107 – 1114.
[150] G. E. Eperon, G. M. Paternò, R. J. Sutton, A. Zampetti, A. A. Haghighirad, F. Cacialli, H. J. Snaith, *J. Mater. Chem. A* **2015**, *3*, 19688 – 19695.
[151] P. Luo, W. Xia, S. Zhou, L. Sun, J. Cheng, C. Xu, Y. Lu, *J. Phys. Chem. Lett.* **2016**, *7*, 3603 – 3608.
[152] Y. Hu, F. Bai, X. Liu, Q. Ji, X. Miao, T. Qiu, S. Zhang, *ACS Energy Lett.* **2017**, *2*, 2219 – 2227.
[153] A. J. Ramadan, L. A. Rochford, S. Fearn, H. J. Snaith, *J. Phys. Chem. Lett.* **2017**, *8*, 4172 – 4176.
[154] Y. Fu, M. T. Rea, J. Chen, D. J. Morrow, M. P. Hautzinger, Y. Zhao, D. Pan, L. H. Manger, J. C. Wright, R. H. Goldsmith, S. Jin, *Chem. Mater.* **2017**, *29*, 8385 – 8394.
[155] L. Protesescu, S. Yakunin, M. I. Bodnarchuk, F. Krieg, R. Caputo, C. H. Hendon, R. X. Yang, A. Walsh, M. V. Kovalenko, *Nano Lett.* **2015**, *15*, 3692 – 3696.
[156] C. Cavallo, F. Di Pascasio, A. Latini, M. Bonomo, D. Dini, *J. Nanomater.* **2017**, *2017*, 5323164.
[157] A. J. Houtepen, Z. Hens, J. S. Owen, I. Infante, *Chem. Mater.* **2017**, *29*, 752 – 761.
[158] X. Lan, S. Masala, E. H. Sargent, *Nat. Mater.* **2014**, *13*, 233 – 240.
[159] Y. Shirasaki, G. J. Supran, M. G. Bawendi, V. Bulovic, *Nat. Photonics* **2013**, *7*, 13 – 23.
[160] G. Nedelcu, L. Protesescu, S. Yakunin, M. I. Bodnarchuk, M. J. Grotevent, M. V. Kovalenko, *Nano Lett.* **2015**, *15*, 5635 – 5640.
[161] G. Xiao, Y. Cao, G. Qi, L. Wang, C. Liu, Z. Ma, X. Yang, Y. Sui, W. Zheng, B. Zou, *J. Am. Chem. Soc.* **2017**, *139*, 10087 – 10094.
[162] A. Voloshinovskii, S. Myagkota, R. Levitskii, *Ferroelectrics* **2005**, *317*, 119 – 123.
[163] S. Dastidar, D. A. Egger, L. Z. Tan, S. B. Cromer, A. D. Dillon, S. Liu, L. Kronik, A. M. Rappe, A. T. Fafarman, *Nano Lett.* **2016**, *16*, 3563 – 3570.
[164] A. Swarnkar, A. R. Marshall, E. M. Sanehira, B. D. Chernomordik, D. T. Moore, J. A. Christians, T. Chakrabarti, J. M. Luther, *Science* **2016**, *354*, 92 – 95.
[165] M. Kulbak, S. Gupta, N. Kedem, I. Levine, T. Bendikov, G. Hodes, D. Cahen, *J. Phys. Chem. Lett.* **2016**, *7*, 167 – 172.
[166] X. Miao, T. Qiu, S. Zhang, H. Ma, Y. Hu, F. Bai, Z. Wu, *J. Mater. Chem. C* **2017**, *5*, 4931 – 4939.
[167] C. F. J. Lau, X. Deng, Q. Ma, J. Zheng, J. S. Yun, M. A. Green, S. Huang, A. W. Y. Ho-baillie, *ACS Energy Lett.* **2016**, *1*, 573 – 577.
[168] X. Chang, W. Li, L. Zhu, H. Liu, H. Geng, S. Xiang, J. Liu, H. Chen, *ACS Appl. Mater. Interfaces* **2016**, *8*, 33649 – 33655.
[169] J. B. Hoffman, A. L. Schleper, P. V. Kamat, *J. Am. Chem. Soc.* **2016**, *138*, 8603 – 8611.
[170] J. B. Hoffman, G. Zaiats, I. Wappes, P. V. Kamat, *Chem. Mater.* **2017**, *29*, 9767 – 9774.
[171] Q. A. Akkerman, M. Gandini, F. Di Stasio, P. Rastogi, F. Palazon, G. Bertoni, J. M. Ball, M. Prato, A. Petrozza, L. Manna, *Nat. Energy* **2016**, *2*, 16194.
[172] S. Panigrahi, S. Jana, T. Calmeiro, D. Nunes, R. Martins, E. Fortunato, *ACS Nano* **2017**, *11*, 10214 – 10221.
[173] C. I. Aguirre, E. Reguera, A. Stein, *Adv. Funct. Mater.* **2010**, *20*, 2565 – 2578.
[174] S. Schünemann, K. Chen, S. Brittman, E. Garnett, H. Tüysüz, *ACS Appl. Mater. Interfaces* **2016**, *8*, 25489 – 25495.
[175] S. Zhou, R. Tang, L. Yin, *Adv. Mater.* **2017**, *29*, 1703682.
[176] R. J. Sutton, G. E. Eperon, L. Miranda, E. S. Parrott, B. A. Kamino, J. B. Patel, M. T. Hörantner, M. B. Johnston, A. A. Haghighirad, D. T. Moore, H. J. Snaith, *Adv. Energy Mater.* **2016**, *6*, 1502458.
[177] S. P. Bremner, M. Y. Levy, C. B. Honsberg, *Prog. Photovoltaics Res. Appl.* **2008**, *16*, 225 – 233.
[178] C. L. Kennedy, A. H. Hill, E. S. Massaro, E. M. Grumstrup, *ACS Energy Lett.* **2017**, *2*, 1501 – 1506.
[179] Q. Ma, S. Huang, S. Chen, M. Zhang, C. F. J. Lau, M. N. Lockrey, H. K. Mulmudi, Y. Shan, J. Yao, J. Zheng, X. Deng, K. Catchpole, M. A. Green, A. W. Y. Ho-Baillie, *J. Phys. Chem. C* **2017**, *121*, 19642 – 19649.
[180] C. Y. Chen, H. Y. Lin, K. M. Chiang, W. L. Tsai, Y. C. Huang, C. S. Tsao, H. W. Lin, *Adv. Mater.* **2017**, *29*, 1605290.
[181] J. K. Nam, M. S. Jung, S. U. Chai, Y. J. Choi, D. Kim, J. H. Park, *J. Phys. Chem. Lett.* **2017**, *8*, 2936 – 2940.
[182] J. S. Niezgoda, B. J. Foley, A. Z. Chen, J. J. Choi, *ACS Energy Lett.* **2017**, *2*, 1043 – 1049.
[183] J. K. Nam, S. U. Chai, W. Cha, Y. J. Choi, W. Kim, M. S. Jung, J. Kwon, D. Kim, J. H. Park, *Nano Lett.* **2017**, *17*, 2028 – 2033.
[184] C. F. J. Lau, M. Zhang, X. Deng, J. Zheng, J. Bing, Q. Ma, J. Kim, L. Hu, M. A. Green, S. Huang, A. Ho-Baillie, *ACS Energy Lett.* **2017**, *2*, 2319 – 2325.
[185] D. Bai, J. Zhang, Z. Jin, H. Bian, K. Wang, H. Wang, L. Liang, Q. Wang, S. F. Liu, *ACS Energy Lett.* **2018**, *3*, 970 – 978.
[186] J. Liang, P. Zhao, C. Wang, Y. Wang, Y. Hu, G. Zhu, L. Ma, J. Liu, Z. Jin, *J. Am. Chem. Soc.* **2017**, *139*, 14009 – 14012.
[187] L. Peedikakkandy, P. Bhargava, *RSC Adv.* **2016**, *6*, 19857 – 19860.
[188] F. Giustino, H. J. Snaith, *ACS Energy Lett.* **2016**, *1*, 1233 – 1240.
[189] B. Saparov, J. P. Sun, W. Meng, Z. Xiao, H. S. Duan, O. Gunawan, D. Shin, I. G. Hill, Y. Yan, D. B. Mitzi, *Chem. Mater.* **2016**, *28*, 2315 – 2322.
[190] B. Lee, C. C. Stoumpos, N. Zhou, F. Hao, C. Malliakas, C. Y. Yeh, T. J. Marks, M. G. Kanatzidis, *J. Am. Chem. Soc.* **2014**, *136*, 15379 – 15385.
[191] D. S. Dolzhnikov, C. Wang, Y. Xu, M. G. Kanatzidis, E. A. Weiss, *Chem. Mater.* **2017**, *29*, 7901 – 7907.
[192] B. Lee, A. Krenselewski, S. Il Baik, D. N. Seidman, R. P. H. Chang, *Sustainable Energy Fuels* **2017**, *1*, 710 – 724.
[193] G. Volonakis, M. R. Filip, A. A. Haghighirad, N. Sakai, B. Wenger, H. J. Snaith, F. Giustino, *J. Phys. Chem. Lett.* **2016**, *7*, 1254 – 1259.
[194] Q. Li, Y. Wang, W. Pan, W. Yang, B. Zou, J. Tang, Z. Quan, *Angew. Chem. Int. Ed.* **2017**, *56*, 15969 – 15973; *Angew. Chem.* **2017**, *129*, 16185 – 16189.

[195] M. Arafat Mahmud, N. Kumar Elumalai, M. Baishakhi Upama, D. Wang, V. R. Gonçales, M. Wright, J. Justin Gooding, F. Haque, C. Xu, A. Uddin, *Sol. Energy Mater. Sol. Cells* **2018**, *174*, 172 – 186.
[196] R. T. Ginting, E. S. Jung, M. K. Jeon, W. Y. Jin, M. Song, J. W. Kang, *Nano Energy* **2016**, *27*, 569 – 576.
[197] M. A. Mahmud, N. K. Elumalai, M. B. Upama, D. Wang, K. H. Chan, M. Wright, C. Xu, F. Haque, A. Uddin, *Sol. Energy Mater. Sol. Cells* **2017**, *159*, 251 – 264.
[198] C. Manspeaker, P. Scruggs, J. Preiss, D. A. Lyashenko, A. A. Zakhidov, *J. Phys. Chem. C* **2016**, *120*, 6377 – 6382.
[199] J. C. Yu, J. A. Hong, E. D. Jung, D. B. Kim, S. M. Baek, S. Lee, S. Cho, S. S. Park, K. J. Choi, M. H. Song, *Sci. Rep.* **2018**, *8*, 1070.
[200] T. Wahl, J. Hanisch, S. Meier, M. Schultes, E. Ahlswede, *Org. Electron.* **2018**, *54*, 48 – 53.
[201] K. C. Icli, M. Ozenbas, *Electrochim. Acta* **2018**, *263*, 338 – 345.
[202] A. Corani, M. H. Li, P. S. Shen, P. Chen, T. F. Guo, A. El Nahhas, K. Zheng, A. Yartsev, V. Sundström, C. S. Ponseca, *J. Phys. Chem. Lett.* **2016**, *7*, 1096 – 1101.
[203] W. Chen, F. Z. Liu, X. Y. Feng, A. B. Djurišić, W. K. Chan, Z. B. He, *Adv. Energy Mater.* **2017**, *7*, 1700722.
[204] A. Mei, X. Li, L. Liu, Z. Ku, T. Liu, Y. Rong, M. Xu, M. Hu, J. Chen, Y. Yang, M. Grätzel, H. Han, *Science* **2014**, *345*, 295 – 298.
[205] T. Leijtens, G. E. Eperon, S. Pathak, A. Abate, M. M. Lee, H. J. Snaith, *Nat. Commun.* **2013**, *4*, 2885.
[206] W. Li, J. Li, G. Niu, L. Wang, *J. Mater. Chem. A* **2016**, *4*, 11688 – 11695.
[207] T. Ye, M. Petrovic, S. Peng, J. L. K. Yoong, C. Vijila, S. Ramakrishna, *ACS Appl. Mater. Interfaces* **2017**, *9*, 2358 – 2368.
[208] G. P. Salvador, D. Pugliese, F. Bella, A. Chiappone, A. Sacco, S. Bianco, M. Quaglio, *Electrochim. Acta* **2014**, *146*, 44 – 51.
[209] M. Gerosa, A. Sacco, A. Scalia, F. Bella, A. Chiodoni, M. Quaglio, E. Tresso, S. Bianco, *IEEE J. Photovoltaics* **2016**, *6*, 498 – 505.
[210] F. Bella, E. D. Ozzello, S. Bianco, R. Bongiovanni, *Chem. Eng. J.* **2013**, *225*, 873 – 879.
[211] M. Imperiyka, A. Ahmad, S. A. Hanifah, F. Bella, *Physica B* **2014**, *450*, 151 – 154.
[212] F. Bella, A. Chiappone, J. R. Nair, G. Meligrana, C. Gerbaldi, *Chem. Eng. Trans.* **2014**, *41*, 211 – 216.
[213] F. Bella, A. Sacco, G. Massaglia, A. Chiodoni, C. F. Pirri, M. Quaglio, *Nanoscale* **2015**, *7*, 12010 – 12017.
[214] F. Bella, S. Galliano, M. Falco, G. Viscardi, C. Barolo, M. Grätzel, C. Gerbaldi, *Green Chem.* **2017**, *19*, 1043 – 1051.
[215] F. Bella, S. Galliano, C. Gerbaldi, G. Viscardi, *Energies* **2016**, *9*, 384.
[216] R. Shanti, F. Bella, Y. S. Salim, S. Y. Chee, S. Ramesh, K. Ramesh, *Mater. Des.* **2016**, *108*, 560 – 569.
[217] F. Bella, A. Lamberti, S. Bianco, E. Tresso, C. Gerbaldi, C. F. Pirri, *Adv. Mater. Technol.* **2016**, *1*, 1600002.
[218] D. Pintossi, G. Iannaccone, A. Colombo, F. Bella, M. Välimäki, K. L. Väisänen, J. Hast, M. Levi, C. Gerbaldi, C. Dragonetti, S. Turri, G. Griffini, *Adv. Electron. Mater.* **2016**, *2*, 1600288.
[219] F. Bella, J. Popovic, A. Lamberti, E. Tresso, C. Gerbaldi, J. Maier, *ACS Appl. Mater. Interfaces* **2017**, *9*, 37797 – 37803.
[220] F. Bella, A. Verna, C. Gerbaldi, *Mater. Sci. Semicond. Process.* **2018**, *73*, 92 – 98.
[221] S. Galliano, F. Bella, G. Piana, G. Giacona, G. Viscardi, C. Gerbaldi, M. Grätzel, C. Barolo, *Sol. Energy* **2018**, *163*, 251 – 255.
[222] R. Sai, K. Ueno, K. Fujii, Y. Nakano, H. Tsutsumi, *RSC Adv.* **2017**, *7*, 37975 – 37982.
[223] R. J. Dillon, L. Alibabaei, T. J. Meyer, J. M. Papanikolas, *ACS Appl. Mater. Interfaces* **2017**, *9*, 26786 – 26796.
[224] G. G. Sonai, A. Tiihonen, K. Miettunen, P. D. Lund, A. F. Nogueira, *J. Phys. Chem. C* **2017**, *121*, 17577 – 17585.
[225] R. Mohammed, G. A. El-Hiti, A. Ahmed, E. Yousif, *Arabian J. Sci. Eng.* **2017**, *42*, 4307 – 4315.
[226] W. Z. N. Yahya, W. T. Meng, M. Khatani, A. E. Samsudin, N. M. Mohamed, *e-Polym.* **2017**, *17*, 355 – 361.
[227] H. J. Peng, J. Q. Huang, Q. Zhang, *Chem. Soc. Rev.* **2017**, *46*, 5237 – 5288.
[228] Y. Guo, J. L. Hou, W. Luo, Z. Q. Li, D. H. Zou, Q. Y. Zhu, J. Dai, *J. Mater. Chem. A* **2017**, *5*, 18270 – 18275.
[229] J. Kreutzer, Y. Yagci, *J. Polym. Sci. Part A* **2017**, *55*, 3475 – 3482.
[230] E. Karaköse, H. Çolak, *Energy* **2017**, *140*, 92 – 97.
[231] V. K. Jayaraman, A. M. Álvarez, M. Bizarro, Y. Koudriavtsev, M. D. L. L. O. Amador, *Thin Solid Films* **2017**, *642*, 14 – 19.
[232] F. Bella, F. Colò, J. R. Nair, C. Gerbaldi, *ChemSusChem* **2015**, *8*, 3668 – 3676.
[233] J. R. Nair, M. Destro, F. Bella, G. B. Appetecchi, C. Gerbaldi, *J. Power Sources* **2016**, *306*, 258 – 267.
[234] L. Porcarelli, A. S. Shaplov, F. Bella, J. R. Nair, D. Mecerreyes, C. Gerbaldi, *ACS Energy Lett.* **2016**, *1*, 678 – 682.
[235] L. Zolin, J. R. Nair, D. Beneventi, F. Bella, M. Destro, P. Jagdale, I. Cannavaro, A. Tagliaferro, D. Chaussy, F. Geobaldo, C. Gerbaldi, *Carbon* **2016**, *107*, 811 – 822.
[236] B. Miccoli, V. Cauda, A. Bonanno, A. Sanginario, K. Bejtka, F. Bella, M. Fontana, D. Demarchi, *Sci. Rep.* **2016**, *6*, 29763.
[237] N. N. M. Radzir, S. A. Hanifah, A. Ahmad, N. H. Hassan, F. Bella, *J. Solid State Electrochem.* **2015**, *19*, 3079 – 3085.
[238] A. Scalia, F. Bella, A. Lamberti, S. Bianco, C. Gerbaldi, E. Tresso, C. F. Pirri, *J. Power Sources* **2017**, *359*, 311 – 321.
[239] F. Bella, A. B. Muñoz-García, G. Meligrana, A. Lamberti, M. Destro, M. Pavone, C. Gerbaldi, *Nano Res.* **2017**, *10*, 2891 – 2903.
[240] F. Colò, F. Bella, J. R. Nair, C. Gerbaldi, *J. Power Sources* **2017**, *365*, 293 – 302.
[241] A. Waleed, M. M. Tavakoli, L. Gu, S. Hussain, D. Zhang, S. Poddar, Z. Wang, R. Zhang, Z. Fan, *Nano Lett.* **2017**, *17*, 4951 – 4957.
[242] P. Ramasamy, D. H. Lim, B. Kim, S. H. Lee, M. S. Lee, J. S. Lee, *Chem. Commun.* **2016**, *52*, 2067 – 2070.
[243] A. Zhang, C. Dong, J. Ren, *J. Phys. Chem. C* **2017**, *121*, 13314 – 13323.
[244] H. Liu, W. Xiang, H. Tao, *J. Photochem. Photobiol. A* **2017**, *344*, 199 – 205.
[245] M. A. Mohamed, M. Abd Mutalib, Z. A. Mohd Hir, M. F. M. Zain, A. B. Mohamad, L. J. Minggu, N. A. Awang, W. N. W. Salleh, *Int. J. Biol. Macromol.* **2017**, *103*, 1232 – 1256.
[246] Y. S. Kim, S. Kriegel, K. D. Harris, C. Costentin, B. Limoges, V. Balland, *J. Phys. Chem. C* **2017**, *121*, 10325 – 10335.
[247] D. Schleicher, H. Leopold, H. Borrmann, T. Strassner, *Inorg. Chem.* **2017**, *56*, 7217 – 7229.
[248] A. Wang, H. Xu, X. Liu, R. Gao, S. Wang, Q. Zhou, J. Chen, X. Liu, L. Zhang, *Polym. Chem.* **2017**, *8*, 3177 – 3185.
[249] A. B. Puthirath, S. Patra, S. Pal, M. Manoj, A. Puthirath Balan, S. Jayalekshmi, N. N. Tharangattu, *J. Mater. Chem. A* **2017**, *5*, 11152 – 11162.
[250] Y. Lin, Y. Cheng, J. Li, J. D. Miller, J. Liu, X. Wang, *RSC Adv.* **2017**, *7*, 24856 – 24863.
[251] E. Singh, K. S. Kim, G. Y. Yeom, H. S. Nalwa, *RSC Adv.* **2017**, *7*, 28234 – 28290.
[252] W. C. Chen, S. Nachimuthu, J. C. Jiang, *Sci. Rep.* **2017**, *7*, 4979.
[253] K. Stalindurai, A. Karuppasamy, J. D. Peng, K. C. Ho, C. Ramalingan, *Electrochim. Acta* **2017**, *246*, 1052 – 1064.
[254] W. J. Mir, M. Jagadeeswararao, S. Das, A. Nag, *ACS Energy Lett.* **2017**, *2*, 537 – 543.
[255] X. Yuan, S. Ji, M. C. De Siena, L. Fei, Z. Zhao, Y. Wang, H. Li, J. Zhao, D. R. Gamelin, *Chem. Mater.* **2017**, *29*, 8003 – 8011.
[256] S. Q. Guo, L. C. Wang, C. G. Zhang, G. C. Qi, B. C. Gu, L. Liu, Z. H. Yuan, *Nanoscale* **2017**, *9*, 6837 – 6845.
[257] H. Liu, X. Zhang, L. Zhang, Z. Yin, D. Wang, J. Meng, Q. Jiang, Y. Wang, J. You, *J. Mater. Chem. C* **2017**, *5*, 6115 – 6122.
[258] W. Liu, K. Zhu, S. J. Teat, G. Dey, Z. Shen, L. Wang, D. M. O'Carroll, J. Li, *J. Am. Chem. Soc.* **2017**, *139*, 9281 – 9290.
[259] J. He, Y. Liu, J. Gao, L. Han, *Photochem. Photobiol. Sci.* **2017**, *16*, 1049 – 1056.
[260] Y. Ye, L. Wang, L. Guan, F. Wu, J. Qian, T. Zhao, X. Zhang, Y. Xing, J. Shi, L. Li, R. Chen, *Energy Storage Mater.* **2017**, *9*, 126 – 133.
[261] K. Zouhri, J. Alsadi, L. Ferreira, M. Chikhalsouk, M. Shinneeb, F. Koudsi, O. Khondker, S. Mohamad, Y. Nimir, *Sol. Energy* **2017**, *155*, 920 – 933.
[262] A. Gavriluta, T. Fix, A. Nonat, A. Slaoui, J. F. Guillemoles, L. J. Charbonnière, *J. Mater. Chem. A* **2017**, *5*, 14031 – 14040.
[263] N. Harankahawa, K. Perera, K. Vidanapathirana, *J. Energy Storage* **2017**, *13*, 96 – 102.
[264] M. Khalili, M. Abedi, H. S. Amoli, S. A. Mozaffari, *Carbohydr. Polym.* **2017**, *175*, 1 – 6.
[265] X. Sheng, Y. Liu, Y. Wang, Y. Li, X. Wang, X. Wang, Z. Dai, J. Bao, X. Xu, *Adv. Mater.* **2017**, *29*, 1700150.

[266] S. Liu, L. Yao, Q. Zhang, L. L. Li, N. T. Hu, L. M. Wei, H. Wei, *Acta Phys. Chim. Sin.* **2017**, *33*, 2339 – 2358.
[267] Y. Y. Li, J. G. Wang, X. R. Liu, C. Shen, K. Xie, B. Wei, *ACS Appl. Mater. Interfaces* **2017**, *9*, 31691 – 31698.
[268] F. W. Low, C. W. Lai, *Renewable Sustainable Energy Rev.* **2018**, *82*, 103 – 125.
[269] D. Zhao, Z. Qin, J. Huang, J. Yu, *Org. Electron.* **2017**, *51*, 220 – 242.
[270] B. Škipina, A. S. Luyt, L. Csóka, V. Djokovic, D. Dudic, *Dyes Pigm.* **2018**, *149*, 51 – 58.
[271] Z. Lin, X. Guo, H. Yu, *Nano Energy* **2017**, *41*, 646 – 653.
[272] Y. J. Huang, C. P. Lee, H. W. Pang, C. T. Li, M. S. Fan, R. Vittal, K. C. Ho, *Mater. Today Energy* **2017**, *6*, 189 – 197.
[273] H. Meier, Z. S. Huang, D. Cao, *J. Mater. Chem. C* **2017**, *5*, 9828 – 9837.
[274] F. Opoku, K. K. Govender, C. G. C. E. Van Sittert, P. P. Govender, *New J. Chem.* **2017**, *41*, 11701 – 11713.
[275] V. I. Tomin, D. V. Ushakou, *Polym. Test.* **2017**, *64*, 77 – 82.
[276] R. Zhang, D. Liu, Y. Wang, T. Zhang, X. Gu, P. Zhang, J. Wu, Z. D. Chen, Y. Zhao, S. Li, *Electrochim. Acta* **2018**, *265*, 98 – 106.
[277] Y. Wu, P. Wang, S. Wang, Z. Wang, B. Cai, X. Zheng, Y. Chen, N. Yuan, J. Ding, W. H. Zhang, *ChemSusChem* **2018**, *11*, 837 – 842.
[278] M. Chen, M. G. Ju, A. D. Carl, Y. Zong, R. L. Grimm, J. Gu, X. C. Zeng, Y. Zhou, N. P. Padture, *Joule* **2018**, *2*, 558 – 570.
[279] G. Zhou, J. Wu, Y. Zhao, Y. Li, J. Shi, Y. Li, H. Wu, D. Li, Y. Luo, Q. Meng, *ACS Appl. Mater. Interfaces* **2018**, *10*, 9503 – 9513.
[280] C. H. Ng, T. S. Ripolles, K. Hamada, S. H. Teo, H. N. Lim, J. Bisquert, S. Hayase, *Sci. Rep.* **2018**, *8*, 2482.
[281] D. Prochowicz, P. Yadav, M. Saliba, D. J. Kubicki, M. M. Tavakoli, S. M. Zakeeruddin, J. Lewiński, L. Emsley, M. Grätzel, *Nano Energy* **2018**, *49*, 523 – 528.

Manuscript received: March 4, 2018
Accepted manuscript online: May 17, 2018
Version of record online: June 27, 2018